11. PIONEER VENUS EXPERIMENT DESCRIPTIONS

edited by

L. COLIN and D. M. HUNTEN

Abstract. This concluding paper of a special issue of *Space Science Reviews*, devoted to the exploration of Venus and the Pioneer Venus Program, contains brief engineering descriptions of the experiments to be integrated into the Orbiter and Multiprobe scientific payloads.

1. Introduction

The expected *scientific* performance of each of the experiments to be incorporated in the Pioneer Venus Orbiter and Multiprobe Missions was discussed in detail in the preceding papers. The *engineering* performance expected is presented in the following collection of short experiment descriptions, prepared by the appropriate Principal Investigator. A total of 114 scientists are officially associated with the Pioneer Venus program (although not members of its PVSSG). The overwhelming majority are, of course, Co-Investigators. A complete list of scientists together with their experiment associations are listed in Table I.

2. Bus Neutral Mass Spectrometer (BNMS) — U. von Zahn/Bonn

2.1. Introduction

This paper describes the design objectives and operational parameters of the gas analyzer carried aboard the Multiprobe Bus. The primary scientific objectives of this experiment are to measure *in situ* the number densities of the various atmospheric constituents and their altitude dependence from about 1000 to 130 km, emphasizing the altitude range which can be reached neither by the entry probes nor the orbiter. From these data the following will be derived: height of the turbopause, approximate eddy diffusion coefficients, neutral atmosphere composition at the ionospheric peak, exospheric temperatures, isotopic ratios, radiogenic noble gas content (^{4}He, ^{40}Ar).

2.2. Design objectives

(a) Provide a measurement capability up to the highest feasible pressures in order to extend the atmospheric investigations as low as possible into the Venus thermosphere.

(b) Provide a measurement capability of reactive gases like O, and of molecules like CO_2 which may break up in the instrument ion source due to their high kinetic energy with respect to the Bus (11 km s^{-1}).

(c) Provide a fast data sampling and telemetering capability to cope with the Bus vertical descent speed of the order of 3 km s^{-1} at 150 km through an atmosphere having a scale height of about 6 km.

Space Science Reviews **20** (1977) 451–525.

TABLE 1 Pioneer venus scientific investigators

Investigator	Organization	Investigation																																					
		Multiprobe																Orbiter																							
		1. S.	2 BNMS	3 BIMS	4 LNMS	5 LGC	6 LSFR	7 LIR	8 LCPS	9 LN, SN	10 LAS, SAS	11 SNFR	12 DLBI	13 MWIN	14 MPRO	15 MTUR	1. S.	16 ONMS	3 OIMS	17 ORPA	18 OETP	19 OMAG	20 OPA	21 OEFD	22 OCPP	23 OIR	24 OUVS	25 ORAD	26 OGBD	27 ORO	28 OGPE	29 OTUR	30 OAD	31 OIDD	32 OCM					
Anderson, Jr., D. E.	U. of Colo.																									C													
Barnes, A.	ARC																					C																	
Barth, C. A.	U. of Colo.																									C													
Bauer, S. J.	GSFC	X		C															C																				
Beer, R.	JPL																								C													
Berry, W.	ARC					C																																	
Blamont, J.	CNES									P																													
Blanchard, R. C.	LaRC										C																												
Boese, R. W.	ARC							P																															
Brace, L. H.	GSFC																			P																		
Brinton, H. C.	GSFC			C															C																			
Brown, W. E.	JPL																										T											
Carignan, G. E.	U. of Mich.																	C																				
Carle, G. C.	ARC					C																																
Chahine, M. T.	JPL																								C													
Cloutier, P. A.	Rice Univ.			C															C																			
Coffeen, D. L.	GISS/SUNY																							C														
Coleman, P. J.	UCLA																				C																	
Colin, L.	ARC																					C																
Collard, H. R.	ARC																																					
Conner, J. P.	LASL																											C										
Counselman, C. C.	MIT												P																									
Coroniti, F. V.	UCLA																					C																
Croft, T. A.	SRI														P														P									
Danielson, G. E.	JPL											C																										
Dickinson, R.	NCAR																								C													
Derr, J.	USGS										C																											
Donahue, T. M.	U. of Mich.	X		C	C												X		C		C																		
Evans, W. D.	LASL																											P										
Farmer, C. B.	JPL																								C													
Fymat, A. L.	JPL											C																										

C = Co-Investigator; P = Principal Investigator; TL = Team Leader; T = Team Member

TABLE 1 Pioneer venus scientific investigators

Investigator	Organization	Investigation																																		
		Multiprobe																Orbiter																			
		1	2	3	4	5	6	7	8	9	10	11	12	13	14	15		16	3	17	18	19	20	21	22	23	24	25	26	27	28	29	30	31	32	
		I. S.	BNMS	BIMS	LNMS	LGC	LSFR	LIR	LCPS	LN, SN	LAS, SAS	SNFR	DLBI	MWIN	MPRO	MTUR		I. S.	ONMS	OIMS	ORPA	OETP	OMAG	OPA	OEFD	OCPP	OIR	OUVS	ORAD	OGBD	ORO	OGPE	OTUR	OAD	OIDD	OCM	
Gille, J. C.	NCAR																									C										
Giver, L. P.	ARC							C																												
Goody, R. M.	Harvard Univ.	X																						C												
Green, I. M.	TRW Systems																																			
Hansen, J. E.	GISS																								P											
Hartle, R. E.	GSFC			C														C	C																	
Herman, J. R.	GSFC			C															C																	
Herman, M.	U. des Sci.Tech.											C																								
Higbie, P. R.	LASL																												C							
Hodges, Jr., R. R.	UTD				C																															
Hoffman, J. H.	UTD				P																															
Hord, C. W.	U. of Colo.																											C								
Houghton, J. T.	U. of Oxford																									C										
Hunten, D. M.	KPNO	X	C						C									C																		
Ingersoll, A. P.	CIT																									C										
Intriligator, D. S.	USC																						C													
Kaula, W. H.	UCLA																											T								
Kawabata, K.	GISS/GTE																								C											
Keating, G. M.	LaRC																																P			
Kennel, C. F.	UCLA																					C														
Kirk, D. B.	ARC										C																									
Klebesadel, R. W.	LASL																												C							
Kliore, A. J.	JPL													P																P					
Knollenberg, R. G.	PMS, Inc.								P																											
Knudsen, W. C.	LMSC																			P															
Kolpin, M. A.	TRW Systems				C																															
Krankowsky, D.	Max-Planck		C																																	
Lacis, A. A.	GISS/GTE																								C											
Lane, W. A.	GISS/GTE																								C											
Lenoble, J.	U. des Sci.Tech.											C																								

C = Co-Investigator; P = Principal Investigator; TL = Team Leader; T = Team Member

TABLE 1 Pioneer venus scientific investigators

Investigator	Organization	Investigation: Multiprobe															Investigation: Orbiter																					
		I. S.	2 BNMS	3 BIMS	4 LNMS	5 LGC	6 LSFR	7 LIR	8 LCPS	9 LN, SN	10 LAS, SAS	11 SNFR	12 DLBI	13 MWIN	14 MPRO	15 MTUR	I. S.	16 ONMS	3 OIMS	17 ORPA	18 OETP	19 OMAG	20 OPA	21 OEFD	22 OCPP	23 OIR	24 OUVS	25 ORAD	26 OGBD	27 ORO	28 OGPE	29 OTUR	30 OAD	31 OIDD	32 OCM
Martonchik, J. V.	JPL																X									C		T								
Masursky, H.	USGS																																				
Mauersberger, K.	U. of Minn.		C																		C															
McElroy, M. B.	Harvard U.				C																															
McGill, G. E.	U. of Mass.																X											T								
McKibbin, D. D.	ARC																					C														
McPherron, R. L.	UCLA																				C															
Michel, F. C.	Rice Univ.			C															C																	
Mihalov, J. D.	ARC																					C														
Miller, J. H.	ARC							C																												
Nagy, A. F.	U. of Mich.																X				C															
Niemann, H. B.	GSFC																	P																		
Nier, A. O.	U. of Minn.		C																																	
Olson, R. A.	LASL																											C								
Oyama, V. I.	ARC					P																														
Pedersen, A.	ESA																				C															
Peskett, G. D.	U. of Oxford																								C											
Pettengill, G. H.	MIT												C														TL						P			
Phillips, R. J.	JPL																																			
Pollack, J. B.	ARC	X				C		C																												
Prinn, R.	MIT												C																							
Ragent, B.	ARC									P																										
Rivas, E. K.	GISS/MIT																							C												
Rodgers, C. D.	U. of Oxford																								C											
Russell, C. T.	UCLA																				P															
Scarf, F. L.	TRW Systems																						P													
Schubert, G.	UCLA																X																			
Seiff, A.	ARC										P																									
Shapiro, I. I.	MIT												C																							P
Siscoe, G. L.	UCLA																				C															
Sommer, S. C.	ARC										C																									

C = Co-Investigator; P = Principal Investigator; TL = Team Leader; T = Team Member

TABLE 1 Pioneer venus scientific investigators

Investigator	Organization	Investigation: Multiprobe															Investigation: Orbiter																			
		I. S.	2 BNMS	3 BIMS	4 LNMS	5 LGC	6 LSFR	7 LIR	8 LCPS	9 LN, SN	10 LAS, SAS	11 SNFR	12 DLBI	13 MWIN	14 MPRO	15 MTUR	I. S.	16 ONMS	3 OIMS	17 ORPA	18 OETP	19 OMAG	20 OPA	21 OEFD	22 OCPP	23 OIR	24 OUVS	25 ORAD	26 OGBD	27 ORO	28 OGPE	29 OTUR	30 OAD	31 OIDD	32 OCM
Spalding, R. E.	Sandia																											C						
Spencer, N. W.	GSFC	X																C																
Spenner, K.	IPW																			C														
Spreiter, J. R.	Stanford U.																			C														
Sromovsky, L. A.	U. of Wisc.											C																						
Stewart, A. I.	U. of Colo.																									P								
Stone, P. H.	GISS/MIT																							C										
Strong, I. B.	LASL																											C						
Suomi, V. E.	U. of Wisc.											P																						
Taylor, F. W.	JPL																								P									
Taylor, Jr., H. A.	GSFC			P															P															
Thomas, G. E.	U. of Colo.																									C								
Tomasko, M. G.	U. of Ariz.						P																											
Travis, L. D.	GISS/GTE																							C										
von Zahn, U.	U. of Bonn		P																															
Whitten, R. C.	ARC																			C			C											
Williamson, E. J.	U. of Oxford																								C									
Woeller, F. H.	ARC					C																												
Wolfe, J. H.	ARC																					P												
Wolfe, W. L.	U. of Ariz.						C																											
Woo, R.	JPL															P														P				
Young, R.	ARC										C																							

C = Co-Investigator; P = Principal Investigator; TL = Team Leader; T = Team Member

(d) Provide a large dynamic signal range to allow measurements over a wide altitude region of minor constituents like N_2, the noble gases and of isotope abundance ratios.

(e) Provide a high confidence level in the absolute values of the measured number densities.

2.3. General instrument design

The BNMS is a double-focusing Mattauch–Herzog electric and magnetic deflection mass spectrometer. Our preference for the double-focusing instrument is based upon its small and compact design, the demonstrated constancy of the sensitivity of such an instrument at high pressures, the possibility of using a multiple collector system (which eases the requirements for dynamic range and yields some inherent redundancy), and the considerable experience which we have in employing this type of instrument in space research (Nier *et al.*, 1973; Trinks, 1975).

The four major parts of the mass spectrometer are shown schematically in Figure 1: ion source, electric and magnetic analyzer, and ion collector system.

The ambient atmospheric particles (1) enter the ion source through high-transparency grids (from the left in Figure 1). Inside the ion box (3) the atmospheric particles are ionized by electron bombardment. The electron beam (4) is emitted from a heated filament, collimated in a magnetic field and collected at the opposite side by a back-up filament. In case of a filament failure the roles of the two are reversed. The ions produced along the electron beam are drawn out of the ion box by the lens (6) onto the object slit (8). In the flythrough mode of the ion source, lens (6) carries a suitable positive potential with respect to the ion box. Thus ions formed with low initial kinetic energy in the ion box cannot penetrate through the ion retarding slit (6), whereas ions with high kinetic energies are able to pass slit (6) (Nier *et al.*, 1974).

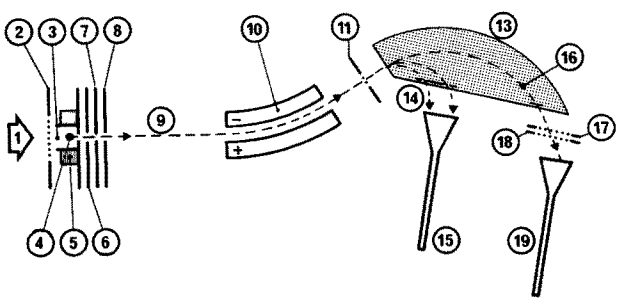

Fig. 1. (BNMS). BNMS sensor schematic. 1 – ambient gas particles: 2 – ion repeller; 3 – ion box; 4 – electron beam; 5 – electron focusing magnet; 6 – ion retarding slit; 7 – ion focusing plates $J+$, $J-$; 8 – object slit; 9 – ion beam; 10 – electric analyzer; 11 – total ion current monitor; 13 – magnetic analyzer; 14 – low mass ion trajectories (1–8 AMU); 15 – low mass multiplier; 16 – high mass ion trajectory (12–46 AMU); 17 – electron suppressor grid; 18 – high mass ion collector; 19 – high mass multiplier.

The ions then enter the electric (10) and magnetic (13) analyzers where energy focusing and mass separation takes place. To collect simultaneously ions of more than one mass number a multiple ion collector system is employed. Three exit slits, but two ion collector systems are used, covering the main ranges 1–18 AMU (low mass collector) and 12–46 AMU (high mass collector). Mass spectra are obtained by varying the electric analyzer and ion accelerating voltages. Ions entering the high mass collector travel in a 3.5 cm radius arc in the magnetic analyzer.

Spiraltron electron multipliers (15, 19) in the counting mode are used as detectors for both the low and high mass ion collectors. A 20% transmission grid (18), mounted between the high mass collector slit and its multiplier detector, intercepts 80% of the beam. It is connected to an electrometer amplifier and thus extends the dynamic range of the measurement when the ion currents are too large for the electron multiplier. In practice there is about one order of magnitude overlap in the range of the two measuring techniques. This permits also a verification of the gain characteristics of the multiplier.

2.4. Special Instrument Features

A titanium sublimation pump and an ion getter pump connected to the analyzer housing maintain a pressure differential of better than 1000:1 between ion source and mass analyzer. In addition, the path length for ions in the high pressure region of the ion source is kept rather short. In this way well behaved spectra and sensitivities are obtained up to ion source pressures of 10^{-2} mbar (see Figure 2). Taking into account the proper ram factor this translates into a measurement capability for ambient number densities of more than 10^{12} cm^{-3} or altitudes as low as 130 km.

The ion source will be operated in the flythrough mode for 25% of the time available at altitudes below about 250 km. The BNMS will be mounted with a 5° offset-angle to the Bus spin axis and hence will experience a periodic modulation

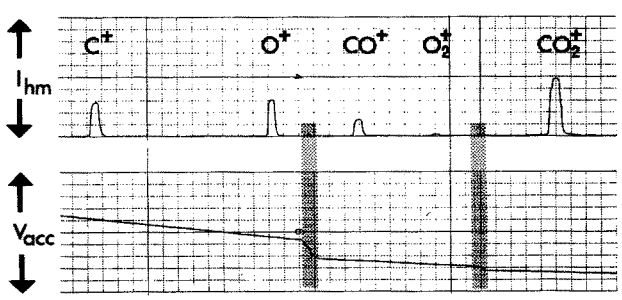

Fig. 2. (BNMS). Example of spectra taken with ion source pressure of 6×10^{-3} mbar CO_2. Upper trace shows ion current registered at high mass ion collector (18) with 1×10^{-8} A full scale for ions of C^+ (12 AMU) till O_2^+ (32 AMU) and with 4×10^{-8} A full scale for CO_2^+ (44 AMU). The lower trace shows the ion accelerating voltage with 2 kV full scale. Mass ranges from 17 to 26 AMU and from 34 to 42 AMU were spared (shaded areas) to compress picture.

of the angle of attack by 10°. By synchronizing the BNMS internal mass programmer with the Bus spin rate and spin phase, flythrough mode data will be collected alternately at minimum and maximum angle of attack. This will allow a verification of the performance of the BNMS in the flythrough mode which, is difficult to evaluate in the laboratory.

During the entry period the instrument will be operated in the peak stepping mode, where only the tops of selected mass peaks and required zero levels will be sampled. Two different measurement programs will be used, one for high and one for low altitudes. All the constituents of major importance will be measured approximately once per second, which provides for a minimum of 2 samples per scale height.

A wide dynamic range of detectable signals is achieved by combining ion-counting multipliers with auto-ranging electrometers and the use of dissociation and isotopic peaks for the measurement of CO_2 at high ion source densities. Furthermore, in the high altitude mode of the mass program the integration time for a single peak top increases with decreasing count rate thus improving the counting statistics for low intensity peaks. The BNMS can thus detect ambient densities from about $10^4\,cm^{-3}$ to above $10^{12}\,cm^{-3}$.

Four design features are provided to ensure high confidence in the absolute values of the measured densities: To protect the stability of the instrument calibration, in the laboratory the ion source cap is attached to the gas analyzer under vacuum inside the calibration system. This avoids exposure of the gas analyzer interior to atmospheric pressure after the main laboratory calibration. An internally preprogrammed test mode allows, upon ground command, the checking of the correct peak position and the gain curve of the two multipliers and the initiation of corrective actions if required. A separate ion collector (11 in Figure 1), intercepting part of the ion beam between electric and magnetic analyzer, will be as a monitor for the total number density in the ion source and allows in-flight checks on the instrument's mass discrimination curve. An in-flight calibration of basic instrument sensitivites will be performed one day before Venus encounter and shortly *before* the ion source cap is ejected; a known amount of gas will be released into the BNMS sensor by breaking a small glass vial. Knowing the total volume of the sensor, the number density inside the sensor can be calculated and used as reference for the final determination of sensor sensitivity.

3. Bus/Orbiter Ion Mass Spectrometer (BIMS/OIMS) — H. Taylor/GSFC

The Ion Mass Spectrometer instruments on the Bus (BIMS) and the Orbiter (OIMS) will measure the composition and concentration of positively charged thermal ions populating the ionosphere of Venus. The instruments will provide continuous, direct measurements of ambient ions encountered between the ionopause and the low altitude limit of approximately 120 km, below which the limitations of aerodynamic heating and ionic mean free path will preclude further

meaningful measurements. During descent through the ionopause and the main body of the Venus ionosphere, the instrument will adaptively repeat measurements of selected positive ions within a mass range including the extremes of 1 AMU (H^+) and 56 AMU (Fe^+).

The measurement concepts of the BIMS/OIMS instruments are closely associated with those established for the instruments flown on the AE-C, E spacecraft (Brinton *et al.*, 1973). The sensor is a Bennett type RF ion mass spectrometer tube, shown schematically in Figure 3. Equations (1) and (2) given in Figure 3 define the measurement relationship between ion mass and parametric grid voltages used in the analysis process, for at rest and spacecraft conditions, respectively. The tube operation is based upon established measurement techniques, described in the literature (Bennett, 1950; Johnson, 1960).

In flight, the sensor is exposed directly to the flux of ambient ions which enter the instrument orifice through the guard-ring grid and are subsequently accelerated along the axis of the spectrometer by a variable negative DC sweep potential (V_a) which is programmed to step and subsequently dwell at voltage levels appropriate for the detection of the particular ion to be resolved. Ions which transit the RF analyzer stages in-phase with the applied voltage V_{RF} gain sufficient energy from RF fields to penetrate the retarding DC field (V_s) and reach the collector region. Ion currents are detected by a dual collector system consisting of a low gain grid collector and a high gain solid disk collector. Collected

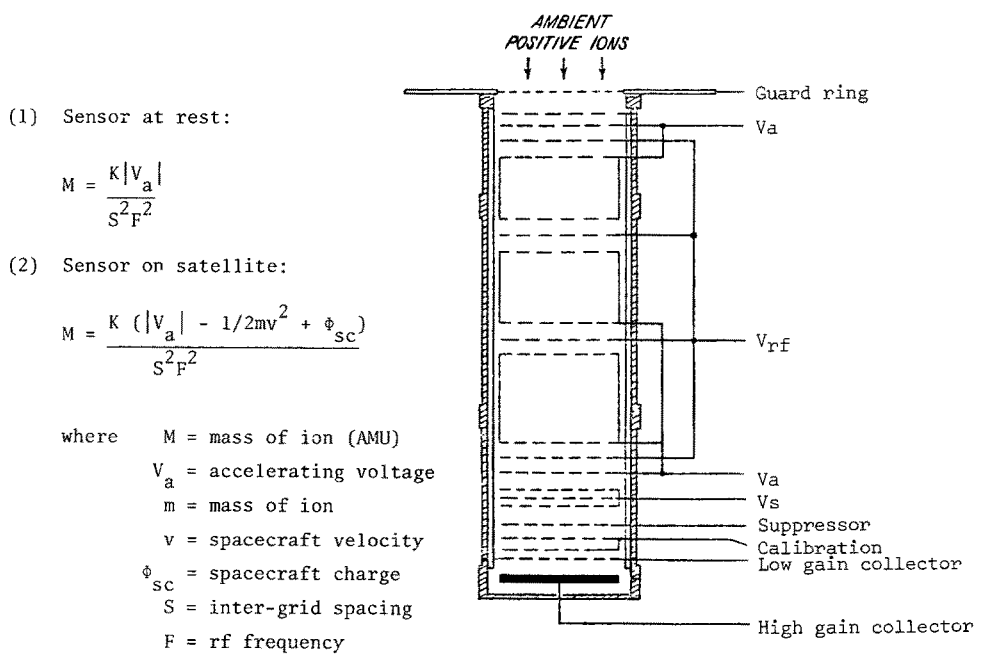

Fig. 3. (OIMS/BIMS). Bennett spectrometer tube and analysis equations.

currents are amplified by an electrometer preamplifier followed by a cascade postamplifier, providing a dynamic range of 10^6 in current sensitivity.

To accommodate mission requirements unique to Pioneer Venus, an automated logic system is used for inflight control of the sensor grid potentials. The logic features two adaptive design techniques, namely the explore–adapt system, and the servo V_s, V_a system. These functions are included in the simplified block diagram of Figure 4.

The basic measurement cycle of 6.3 s is composed of an explore interval of approximately 1.8 s followed by an adapt interval of approximately 4.5 s. During the explore interval, a search is made for the presence of a maximum of 16 possible ion species. During the adapt interval, repetitive measurements are made of as many as 8 most prominent ions detected during the explore cycle. In this way, the explore–adapt circuit automatically regulates the time rate of measurements of individual ions according to the ion composition encountered.

The servo V_s, V_a system provides automatic in-flight regulation of the analysis and detection of the incoming ions, which in addition to their inherent mass characteristics, exhibit effects related to (1) spacecraft velocity, (2) spacecraft skin charge, and (3) thermal plasma motion. The function of the V_s, V_a servo is to adjust automatically the BIMS/OIMS to operate at constant efficiency and mass resolution, accomodating these external effects. Internally programmed small variations of the amplitudes of V_s, V_a are performed during the dwell of V_a at each mass position. The resulting modulation of the detected ion current is analyzed to identify and subsequently (with servo feedback control) provide the necessary adjustments of the parametric grid voltages to compensate for the effects of spacecraft charge and velocity.

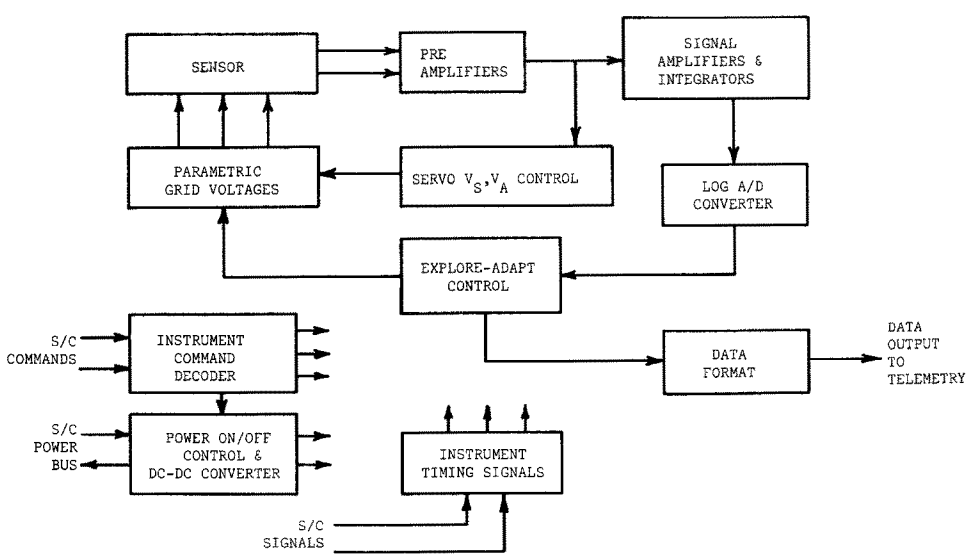

Fig. 4. (OIMS/BIMS). BIMS/OIMS simplified block diagram.

TABLE II
BIMS/OIMS Characteristics

Mass range	Explore scan: 1, 2, 4, 8, 12, 14, 16, 17, 18, 24, 28, 30, 32, 40, 44, 56 AMU Adapt scan: Most prominent detected in explore (8 max.)
*Sampling rate	Explore–adapt cycle = 6.3 seconds Explore scan = 1.8 seconds Adapt scan = 4.5 seconds Minor ions: 1 Sample/6.3 seconds Prominent ions: 6 samples/6.3 seconds (min) *Bus (entry), Orbiter (periapsis)
Resolution	Adjacent ions in selected AMU sequence measured with <1% overlap
Sensitivity	Max: 5×10^6 ions cm^{-3} Min: 5×10^0 ions cm^{-3}
Accuracy	Ion concentration accurate within 10%
Commands	Power on, off + 4 discrete
Modes	On, off —guard ring on, *off —*explore only Calibrate on —servo override *on, off —adapt 8, *4, or *2 *To be exercised on OIMS only
Data outputs	Data line: Bus / Orbiter — Output B_a / N_a: Ion currents, AMU codes B_b / N_b: Servo coefficients B_c / N_c: Instrument monitors B_d / N_d: Instrument monitors

In the case of the Orbiter Mission, the OIMS will include commandable modes for regulating the explore–adapt logic circuit to reduce the number of prominent ions for adaptive repeats from 8 to 4 or 2, with the further option of an explore-only mode. In the case of the Bus, mission constraints prohibit the use of mode commanding, and the BIMS instrument will operate exclusively in the explore–adapt (8/16) mode. Otherwise the BIMS and OIMS instruments are identical. Interface characteristics of the instruments are summarized in Table II.

4. Large Probe Neutral Mass Spectrometer (LNMS) — J. Hoffman / UTD

4.1. Introduction

The large probe mass spectrometer is designed to measure the composition of the neutral atmosphere from parachute deployment (~67 km) to the surface. Wide dynamic and mass ranges are required to survey the atmospheric gases and determine the cloud composition. Special care must be taken in sampling the atmosphere to ensure that chemically active species are not altered by the apparatus.

Key features of the instrument are:

(a) Sample collection through a chemically passive inlet leak that ensures no significant chemical modification of the sample composition.

(b) Variable speed chemical pump system which maintains essentially constant ion source pressure thereby utilizing the instrument's full dynamic range over the entire descent time.

(c) Multi-energy ion source to take advantage of energy dependent cracking patterns in the identification of gases.

(d) High performance mass spectrometer having mass resolution of spectral peaks out to 208 AMU and the capability of detecting minor constituents in the 1 ppm range.

(e) Onboard data processing to permit efficient telemetry of the mass spectra so that atmospheric stratification in the sub-scale height range can be resolved.

(f) Isotopic Ratio Measurement Cell (IRMC) for enriching the non-reactive gas content of a high altitude atmospheric sample, enabling subsequent determination of the inert gas isotopic ratios.

4.2. Instrument description

The mass spectrometer system consists of an instrument mounted inside the large probe pressure vessel with a gas inlet leak that protrudes through the vessel wall out into the atmosphere which is streaming past the probe as it settles toward the planet's surface. Table III gives a summary set of instrument parameters.

The instrument is packaged in two units on a single baseplate mounted on the lower shelf of the probe. One package contains the mass analyzer, ion source, pumping systems, IRMC and associated vacuum valves and plumbing; the adjacent package contains the electronics. The inlet leak, a small pressed tube, penetrates the pressure vessel through a flange 13° below its equator. The tip of the leak lies outside the boundary layer in the free streaming atmosphere to prevent ingestion of spacecraft generated materials. A breakseal cap protects the leak prior to entry into the Venusian atmosphere.

Atmospheric gases and vapors are sampled through the leak and pass into the ion source which is pumped by a getter through a variable conductance orifice valve. This valve is gradually opened by increasing atmospheric pressure as the probe descends, so that a nearly constant pressure is maintained in the ion source.

The gas inlet system has been designed with an extremely small dead volume to minimize the residence time of gas samples within it. Hence, its response time is sufficiently rapid to follow sub-scale height variations in atmospheric composition. Periodic operation of an ion pump eliminates any accumulation of inert gases in the ion source cavity.

Analysis of the gas sample is accomplished by a magnetic sector field mass spectrometer, whose mass range extends from 1 AMU to 208 AMU with resolution sufficient to separate the mercury isotopes and a sensitivity sufficient to detect minor constituents in the 1 ppm range. The ionizing electron energy is stepped

TABLE III

Large probe neutral mass spectrometer

Instrument Parameters	
Instrument:	Sector field mass spectrometer. Mass range: 1 to 208 AMU (2 ranges). Sensitivity: 1 ppm of CO_2. Dynamic range: 10^7. Ion Source: Multi-energy electron impact. Detector: Electron multiplier-ion counting system. Spectral scan time: 64 s.
Inlet System:	Ceramic Micro-Leak Passivated stainless steel leak. Small dead volume-rapid response to changing atmosphere. Variable conductance orifice valve. Chemical pump. Ion pump for rare gas removal.
Isotope Ratio Measurement Cell:	Collects high altitude atmospheric sample. Purges it of active gases (CO_2, H_2, O_2, etc.). Concentrated inert gases admitted to ion source for isotopic ratio measurements.
Telemetry Bandwidth:	Science data: 40 bits per second (10 minor frame words). Status word: 1 minor frame word. Housekeeping: 1 minor frame word (analog).
Commands:	Power command. Quantitative command (from bus). Four discrete commands (from probe).
Mount:	Instrument package on forward instrument mounting shelf. CML penetrates pressure vessel 13° below equator.

through three levels to provide spectral data on the energy dependent cracking patterns of gas samples to aid in the identification of unknown substances and the separation of parent peaks from fragmentary ions.

Measurements are made relative to CO_2. With a 10^7 dynamic range and constant ion source pressure, the 1 ppm sensitivity is maintained over the entire descent time.

Figure 5 is a functional block diagram of the instrument showing the mass spectrometer, power supply and control circuits.

A microprocessor intelligence unit controls the mass scan mode, ion source energy sequence, data accumulation and formatting. The mass spectrum is scanned in 64 s using a peak stepping mode. Accumulated counts for each spectral peak are converted into 10 bit, base 2, floating point numbers. A data rate of only 40 bps is required to transmit the mass spectral data to Earth. Prior to release from the bus, the instrument is ground controlled by a quantitative command (16 bits) for checkout tests. After release, pre-entry and entry commands from the

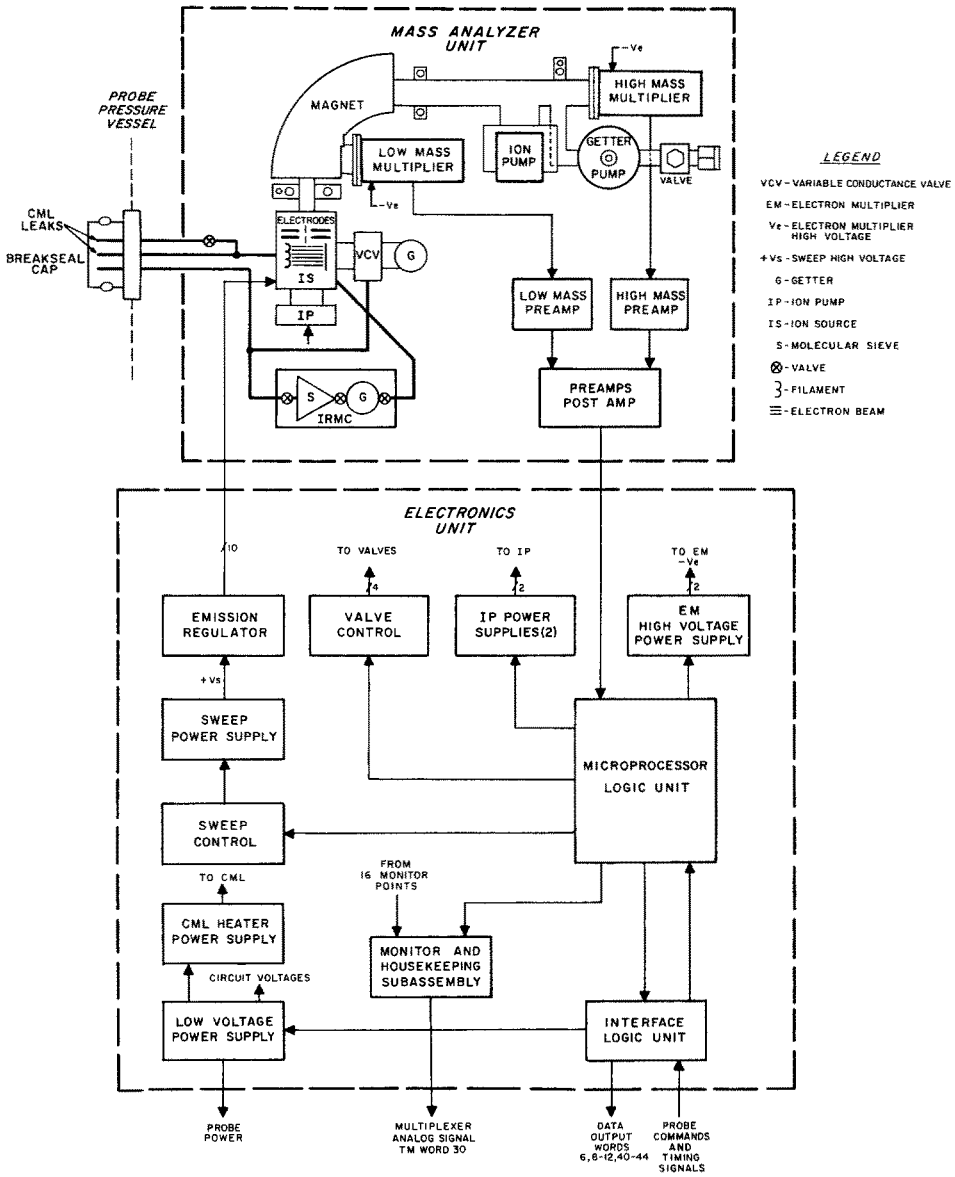

Fig. 5. (LNMS). LNMS functional block diagram.

probe sequencer control the micro-processor which governs the instrument operation.

Approximately 60 mass spectra are expected during descent, from which atmospheric gas densities relative to CO_2 and the structure of the Venusian atmosphere will be obtained. Identification of the vapors from which the clouds are condensed is an important result expected from this experiment.

An atmospheric sample is collected in a small chamber, known as the Isotopic

Ratio Measurement Cell (IRMC), shortly after parachute deployment. This chamber purges the sample of CO_2 and other active gases, leaving an enriched inert gas sample. Just prior to parachute release, where descent speed is at a minimum, the ion source cavity is pumped out and this sample is analyzed for isotopic ratios of the rare gases.

The mass spectrometer system will be calibrated prior to flight using a Venus atmosphere simulator and a number of test gases and vapors. Post flight synthesis of results using the simulator will ensure an accurate interpretation of the data in terms of identification of trace constituents in the Venus atmosphere. Accuracy of measurement is anticipated to be of the order of ±20%.

5. Large Probe Gas Chromatograph (LGC) — V. Oyama / ARC

5.1. Introduction

The Pioneer Venus Gas Chromatograph is a modified version of the gas chromatographic portion of the Viking Biology Gas Exchange Experiment (Oyama, 1972) for Venus atmospheric analysis in a changing large-probe environment.

5.2. Function description

The LGC measures gases that are probable constituents of the Venus atmosphere. Knowledge of their actual abundances will help answer specific questions about the evolution, structure, and thermal balance of Venus. The LGC measures Ne, H_2, N_2, O_2, Ar, CO, CH_4, Kr, CO_2, NH_3, H_2O, H_2S, COS, and SO_2. Other gases such as NO, N_2O, HCl, HBr, C_2H_2, C_2H_6, and SO_3 may also be detected.

At three points during descent of the large probe, atmospheric samples are injected into the helium carrier gas stream. During acquisition of the third sample, two Freons are added to the atmospheric sample. These serve as internal standards. The carrier gas stream branches into two separating chromatographic assemblies which split the atmospheric sample. Resolution of the gases from Ne to CO_2 is attained on the longer of two columns, whereas resolution of the gases from CO_2 to SO_2 is attained on the shorter column. The gases elute from a separating column and pass through one leg of a thermal conductivity detector (TCD). The thermal conductivity differences between the separating carrier gas and a reference carrier gas are transduced into an analog electrical feedback signal. The analog signals are processed by an analog–digital converter to provide the proper signal level for transmission.

5.3. Sampling system

After appropriate sequential actuation of the thermal isolation valves (Figure 6), sampling is accomplished during descent through the Venus atmosphere. Atmospheric gases driven by increasing descent pressures flow through the inlet, through the gas sample loop into the plenum. The plenum and loop provide a linear velocity of $\sim 10\ \mathrm{cm\ s^{-1}}$ through the loop for at least 8 min before each injection. Sequencing of the miniature latching valves injects the sample.

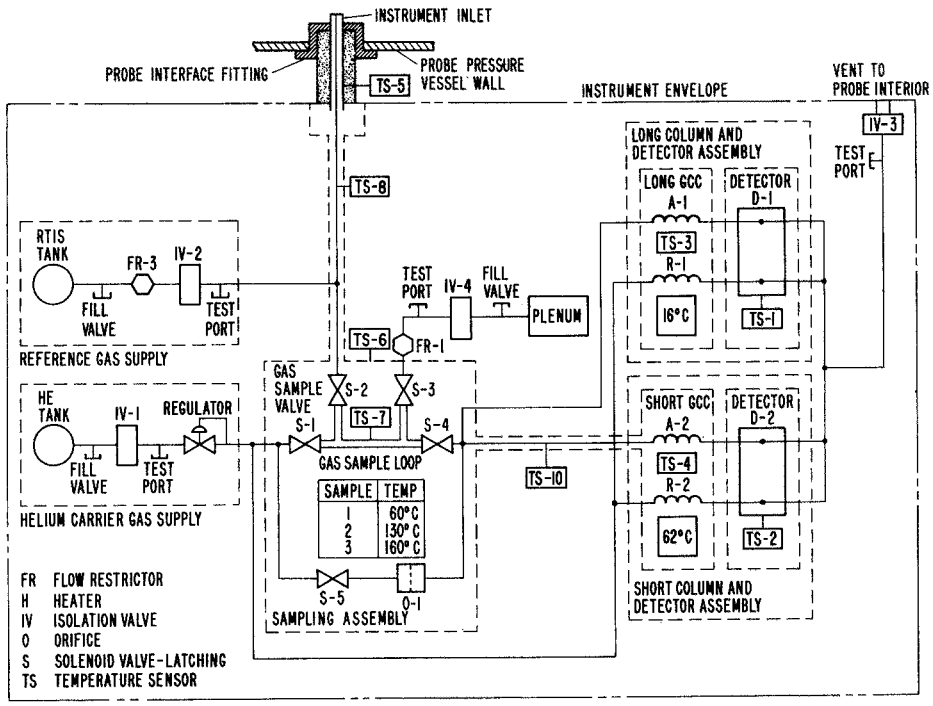

Fig. 6. (LGC). Pioneer Venus gas chromatograph atmospheric analyzer mechanical subsystem (MSS) schematic diagram.

5.4. Chromatographic columns

The long-column assembly consists of a matched pair of packed columns bifilarly wound. The columns (1585 cm long × 0.11 cm i.d.) contain 3.0 g of 100/120 mesh Porapak N (a polystyrene product of Van Waters Assoc.) and are operated at 16°C. Temperature is controlled by a heater surrounded by a shell filled with frozen phase-change material, *n*-pentadecane (m.p. 10°C).

The short-column assembly consists of a pair of columns, similarly wound and mounted. These columns are 244 cm long with a 0.11 cm internal diameter, and contain a prepared polymer mixture of 80%. poly-divinyl benzene and 20% ethylvinylbenzene of 180/220 mesh spheres. The operating temperature is 65°C which is above the large-probe environment during descent. The detector is enclosed by the cylindrical aluminum housing, a cover, and a spacer to form a uniformly heated oven.

5.5. Carrier gas regulation and flow

Helium pressure is regulated at 17.58 kg cm^{-2} referenced to the large probe interior. The flows through all columns will be ~40 standard cubic centimeters min^{-1}.

5.6. Electronic subsystem (ESS)

The LGC data stream begins at the thermal conductivity detectors. The detector block contains two thermistor beads maintained at a few degrees above the surrounding column by a closed loop temperature control system in the low-level electronics (LLE) (Figure 7). If the active thermistor bead changes temperature because of a change in its thermal environment, an error signal is generated. The error signal is then applied to drive the temperature of the bead back to the isothermal value. Thus, the amplified error signal is a measure of the thermal conductivity of the gas flowing past the active thermistor bead. A reference thermistor with its own feedback controller cancels out the effect of temperature and flow variations.

The amplified error signals are summed into a difference amplifier and filtered. The nearly six decades of data range at 1% accuracy is possible using three gains: 997, 71.6, and 4.56. The overall gains are controlled by the A/D converter. The LLE output is reset to +0.75 mV at the beginning of each analysis.

The LLE feeds the 11-bit dual-slope A/D converter. At a command from the data sample rate logic, the A/D converter samples at the highest then at lesser gains until the conversion is within range; then the A/D converter sends a 14-bit word (comprising 11 data bits, 1 column identifier bit, and 2 range bits) to the buffer memory.

The buffer memory (2048 bits) is organized on a first-in-first-out basis. Data are taken out of the memory in 56-bit bytes (4 LGC data words) upon receipt of the read envelope and read clock from the probe.

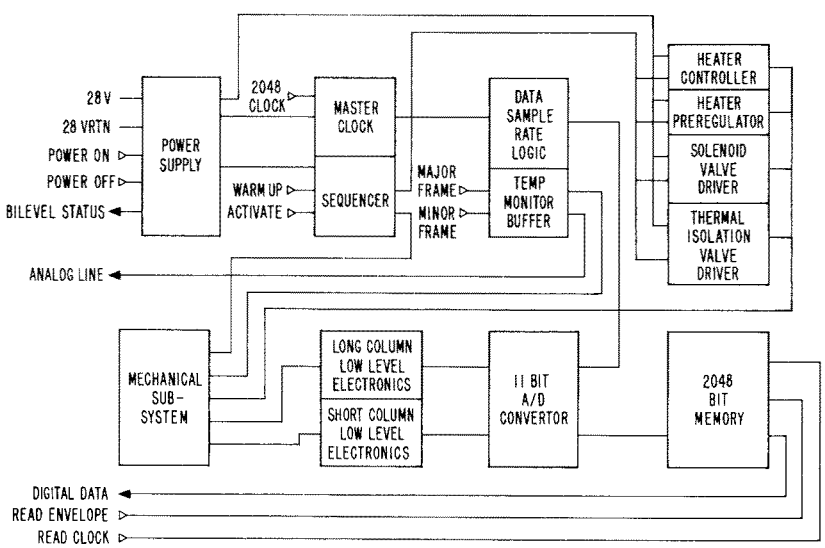

Fig. 7. (LGC). Pioneer Venus gas chromatograph atmospheric analyzer electronic subsystem (ESS) block diagram.

5.7. Performance characteristics

The third sample at the highest pressure contains the maximum number of molecules for analysis. The calculated data in Table IV show the minimum detectable (ppm) at this sampling point.

TABLE IV

Predicted minimum detectable concentration of some selected gases at the third sampling point[a]

Data from breadboard Long-column assembly		Data from laboratory Short-column assembly	
Gas	PPM[a]	Gas	PPM[b]
Ne	2.1		
H_2	32	NH_3	50±40
N_2	0.88	H_2O	50±40
O_2	1.3	H_2S	15
Ar	2.3		
CO	2.4	COS	18
CH_4	6.4	SO_2	61
Kr	5.9		

[a] Sample 3 taken at 18 bars pressure with 350 μl sample loop at 160°C. Sample split equally for long and short columns.

[b] Based upon a signal twice that of the noise of equipment actually used. Uncertainties for NH_3 and H_2O are based upon non-ideal sampling conditions and projections for a better flight system.

6. Large Probe Solar Flux Radiometer (LSFR) — M. Tomasko/Ariz.

The primary goal of the solar flux radiometer (LSFR) aboard the large probe is the measurement of the deposition of solar energy throughout its descent through the atmosphere. These measurements determine the amount of solar energy which reaches the ground and contributes directly to its high temperature through the greenhouse effect and the amount absorbed in the clouds which may contribute to the high surface temperature in a more indirect way.

The solar energy absorbed within a layer of the atmosphere is the difference in the net solar flux entering through the top of the layer and the net flux leaving through the bottom. The net flux F_n, is defined by

$$F_n(h) = \int_{\lambda_1}^{\lambda_2} \int_{-1}^{+1} \mu \int_{0}^{2\pi} I(h, \phi - \phi_0, \mu, \lambda)\, d\phi\ d\mu\ d\lambda$$

where h is the height above the surface, μ is the cosine of the zenith angle, $\phi - \phi_0$ is the azimuth angle measured from the solar azimuth, and λ_1 and λ_2 are the wavelength limits within which most of the solar energy is contained.

In order to avoid having the probe itself or its parachute in the field of view of the LSFR, this instrument samples the intensity field in narrow (~5°) fields of view at a selected set of azimuth and zenith angles. The integrals over solid angle are performed on the ground from the intensity samples. The instrument operates in two modes. In the first portion of the descent when azimuth variation is anticipated, the instrument detects the intensity peak at the solar azimuth and uses the times of successive peaks to control Mode 1 azimuth sampling as given in Table V. If no peaks are detected for more than 16 s, the instrument automatically switches to Mode 2 operation where samples are collected at each zenith angle as frequently as the telemetry rate will allow (every 8 s) corresponding to a vertical resolution of 300 m or better. The vertical resolution in Mode 1 is better than 800 m. In addition, the instrument is locked into Mode 2 at about 54 km altitude (8 min after turn on) to prevent noise at the lower signal levels from triggering mode changes.

The Mode 1 azimuth samples are collected at gaussian quadrature points relative to the Sun. This quadrature scheme contributes less than 1% error in the azimuth integrals for optical depths of 2 or greater.

The zenith angle samples in both instrument modes comprise a two-point Gaussian quadrature for the upward flux and a separate three-point Gaussian quadrature for the downward flux. This scheme introduces only a few percent error in the up and down fluxes at optical depths between 1 and 8 and negligible error at greater optical depths.

Unlike the solid-angle integrals, the integral over wavelength is performed directly by the instrument. Two broad and flat spectral channels are included at

TABLE V

Sampling of the solar radiation field by the solar radiometer

Zenith angle	Mode 1 Azimuth angle measured from the azimuth of the Sun						Mode 2
	0	12	24	60	120	138	
27.5			VIS		VIS		VIS
			IR		IR		IR
	VIS	VIS		VIS		VIS	VIS
60.0	IR	IR		IR		IR	IR
	NB	NB		NB		NB	NB
83.5			VIS		VIS		VIS
			IR		IR		IR
102.2			VIS		VIS		VIS
			IR		IR		IR
			VIS		VIS		VIS
142.1			IR		IR		IR
			NB		NB		NB

VIS = 0.4 to 1.0 μm. IR = 1.0 to 1.8 μm. NB = 0.6 to 0.65 μm.

each azimuth and zenith sample. One filter extends from 0.4 to 1 μm and the other from 1.0 to 1.8 μm. Together they include some 83% of the incident solar energy.

In addition to the two broad filters, a narrower filter from about 0.6 to 0.65 μm is included on one of the upward-looking zenith samples and on one of the downward-looking sample points. Data from this spectral channel can be inverted to yield the single scattering albedo and the optical depth of the clouds throughout the descent.

The LSFR thus includes five small quartz lenses (~3 mm diameter) inside five flat sapphire windows in the pressure vessel. These lenses collect the light at the five zenith angles of Table V. At the focus of each of these lenses is one end of a 3.18 mm diameter quartz rod which contains an aperture stop limiting the field of view to 5 degrees. The rods carry the light past several centimeters of insulation to the cooler detector array. At this end of each rod is a filtered germanium and either one or two filtered silicon detectors having nearly uniform responsivity over their range. The detectors are mounted on a common substrate and are in intimate thermal contact with a mass of $LiNO_3$–$3H_2O$ which absorbs heat upon melting at 30°C in order to stabilize the temperature of the detectors during the descent. In addition, a thermistor is mounted on the detector array and the temperature of the detectors is monitored. The 'detector head' consisting of

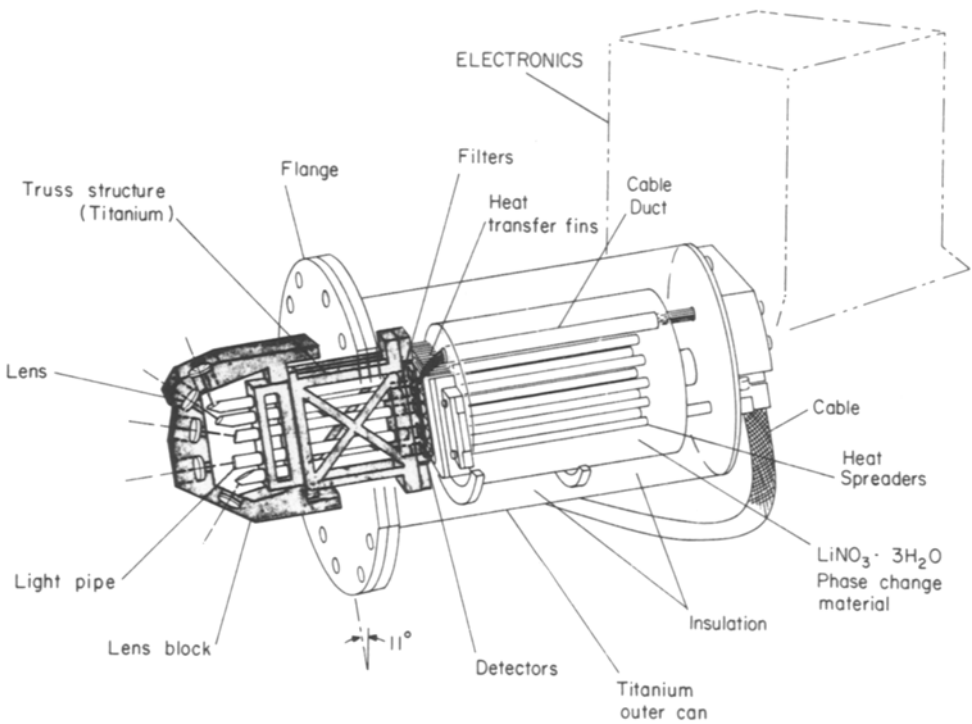

Fig. 8. (LSFR). Drawing of the detector head of the Solar Flux Radiometer.

lenses, quartz rods, filters, detectors, phase change material, and supporting structure is shown in Figure 8.

The outputs from the 12 electronic channels of the detector head are carried to a nearby electronic processing package whose temperature is monitored by a second thermistor. The electronics package includes 12 logarithmic amplifiers, a peak detector circuit, an analog-to-digital data converter, a multiplexer, data buffers, a power supply, and logic circuitry to control sample timing, switching between modes (based on the detection of solar peaks) and activation of a calibrator circuit.

The electronic calibration consists of using precision resistors to superimpose a known current on the 'sky' input current from the detector head once every 16 measurement sets (about every 2 min) during the descent when in mode 2. Absolute radiometry will be possible to an accuracy of several percent, while relative accuracy between upward and downward channels should be possible to about 1% over most of the measurement range.

7. Large Probe Infrared Radiometer (LIR)—R. Boese / ARC

The LIR is designed to measure the divergence of the thermal flux, detect clouds and determine their infrared opacity, and detect the presence of water vapor (and an estimate of its abundance) during descent through Venus' atmosphere.

A schematic configuration of the LIR is given in Figure 9 which also indicates that the instrument is conveniently composed of two sections – the optical head and the electronic box. The electronics box, which is $6.9 \times 5.1 \times 4.2$ in ($17.5 \times 13.0 \times 10.7$ cm), will be of magnesium, where possible, for lightness. The optical head extends 3.0 in (7.6 cm) from the electronics box; the diameter of the phase change chamber is 2.4 in (6.1 cm). The instrument will be located on the aft side of the forward shelf and will view Venus' atmosphere through a type IIa diamond window. The window will be heated to prevent contamination during descent through clouds and will provide an unobstructed $25° \times 25°$ field-of-view centered at 45° upward and downward from the probe horizontal.

The electronics box, in addition to conditioning the raw power from the spacecraft bus, provides closely regulated voltages for several critical items within the instrument. Additionally, the signal conditioning, i.e., amplification, integration, and A/D conversion are performed in this section of the instrument. Control of data acquisition timing, and of calibration sequencing is also accomplished, as is sub-commutation of critical instrument parameters such as component temperatures, calibration source temperatures, and voltage levels. The component parts of the optical head are discussed below.

The detectors selected for this experiment are of the pyroelectric type since they have uniform sensitivity throughout the infrared and do not require coolant for proper operation. The detectors themselves have a slight positive thermal coefficient so should operate slightly better in the warm environment of the large

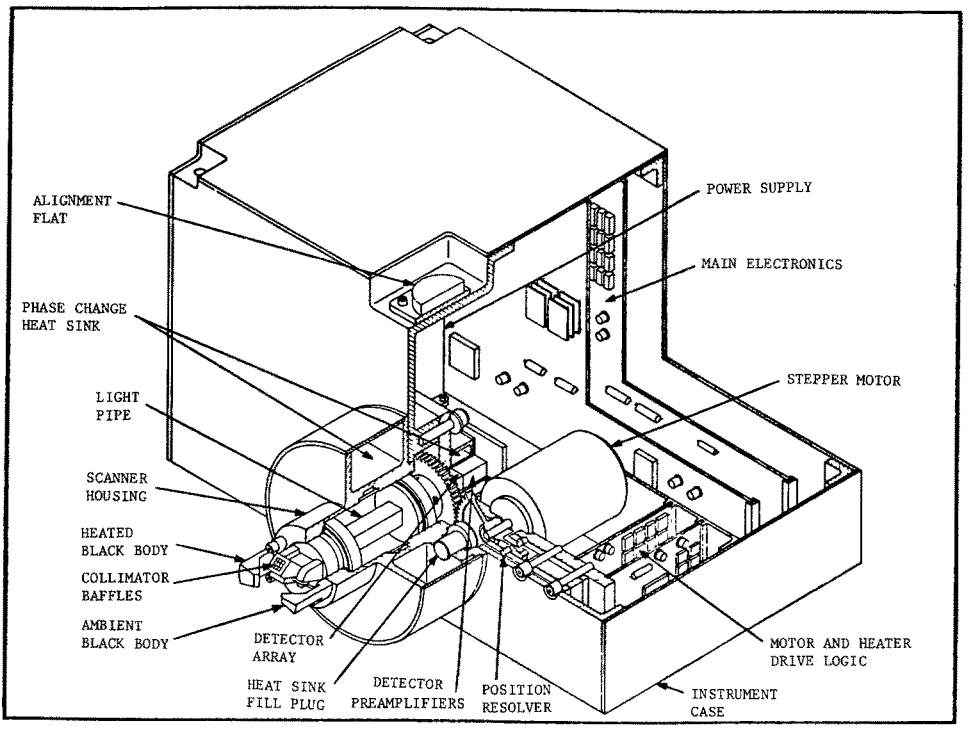

Fig. 9. (LIR). Schematic configuration of Infrared Radiometer.

probe. However, the FET preamplifiers, which are closely coupled to the detectors, degrade by about a factor of two for each 10°C temperature increase. Thus, the entire package is surrounded by phase change material in order to maintain a relatively constant temperature. Each of the six detectors in the package views Venus atmosphere through a different filter: the filters were selected to both accomplish the objectives of the experiment and to assist in monitoring system performance. The filter bandpasses are given in Table VI. Channel A will permit measurement of the net thermal flux, channels B and C will determine the presence of H_2O and estimate its abundance, and channel D will determine cloud opacity. Channel E will, since it is centered in a strong CO_2 band, permit determination of contamination on the outer surface of the window, i.e. the window is transparent to this wavelength radiation but Venus' atmosphere is opaque. Channel F is centered in the lattice vibration band of the type IIa diamond window and thus will permit a determination of window temperature uniformity as the detectors' views are directed first upward and then downward. The output from these last two channels should be zero, within the system noise limits; deviations from zero will indicate a potential problem and thereby also indicate that corrections to the data may be in order.

Radiation from Venus' atmosphere reaches the detector-filter package via the light pipe extenders (A in Figure 10), the moving light pipe (B in Figure 10), and

TABLE VI

Channel	Cut-on Wavelength (microns)	Cut-off Wavelength (microns)
A	3.0	>50.0
B	6.0	7.0
C	7.0	8.0
D	8.0	9.0
E	14.5	15.5
F	4.0	5.0

the stationary light pipe (C in Figure 10). Use of all reflective surfaces minimizes the spectral characteristics which would be imparted by refractive optics, and the light pipe concept essentially eliminates stray radiation from reaching the detectors. The moving light pipe is driven by a geared stepper motor and contains a collimator whose geometry limits the field-of-view of the instrument to 25°×25°. A diffusing element is included in the light pipe chain so that the views of each detector are as nearly identical as possible.

The instrument has its own self-contained calibration system. This consists of two black bodies operating at different temperatures. The temperature difference is sufficient so that a signal-to-noise ratio of at least 100:1 will be generated in all detector–filter channels. The internal sequencing will command the instrument into this mode approximately 6% of the time during descent in order that the overall system performance can be evaluated. The black bodies are located at 90 degrees from the up-down movable light pipe positions as indicated in Figure 9.

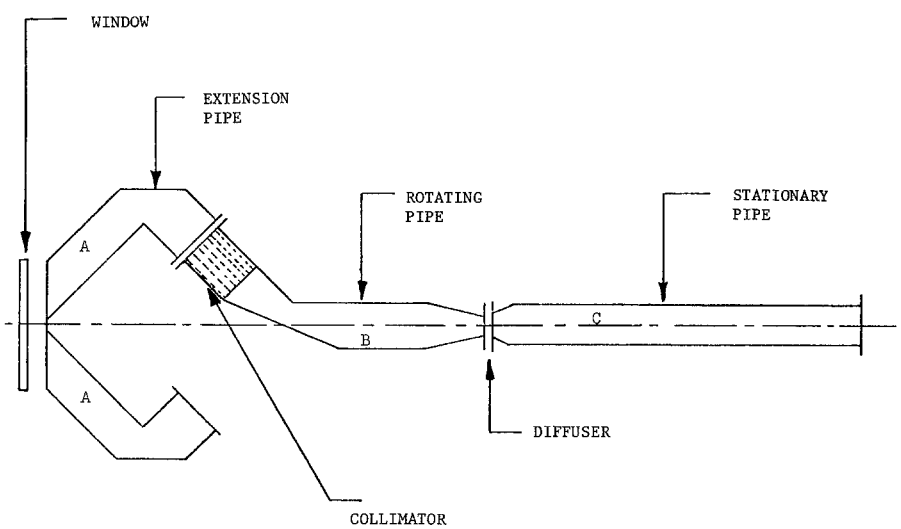

Fig. 10. (LIR). Detector–filter package of Infrared Radiometer.

During descent through Venus' atmosphere the instrument will operate as follows. Net flux measurements will begin as soon as the instrument is commanded on at about 67 km altitude. The up–down flux difference will be obtained at a 2 HZ scan rate and will be integrated for about a 6 second period. (The integration period is established by the data bit rate assigned to the experiment and the dynamic range which must be covered.) The digitized data are then transmitted to Earth during the next integration period. Sampling of Venus atmosphere will continue for 174 s; the instrument will then enter the calibrate mode of operation. After 12 s of radiation calibration and 6 s of electronic calibration, the instrument will again view Venus' atmosphere. The sequence will continue until impact on the planet's surface.

The vertical resolution of Venus' atmosphere (i.e., one integration period) will vary from about 250 m at the top of the atmosphere to about 90 m near the surface. The instrument's sensitivity is such that a signal-to-noise ratio of one is obtained with a net flux difference of about 0.25 W m^{-2}.

8. Large Probe Cloud Particle Size Spectrometer (LCPS)
R. Knollenberg/PMS

The LCPS will measure the particle size and number density in the clouds and lower atmosphere of Venus as a function of altitude. This instrument is an *in situ* measuring device capable of particle size measurements in the range of 0.5–500 μm. The LCPS will be capable of making single particle size measurements at high concentrations (10^3 to 10^4 cm^{-3}) and is relatively insensitive to particle shape and orientation. The LCPS will also be capable of measuring gross particle aspect ratio (length/width). The LCPS will provide a vertical profile of particulate concentration for 34 size classes from 0.5–500 μm. The levels of cloud will be resolved to at least ±400 m. The measurements will be initiated at 67 km and continue to the planetary surface. Aspect ratio measurements for particles 50–500 μm in size will have a resolution of from 1:1 to 10:1.

The prime LCPS measuring technique employed is that of an optical array spectrometer. This technique covers particle sizes from 5–500 μm in sequential ranges of 5–50, 20–200 and 50–500 μm, utilizing multiplexed photodiode arrays. Each size range has ten size classes of equal size width. A scattering subrange will also be operated using one of the light paths of the optical array spectrometer to measure particle sizes from 0.5–5 μm. The optical array spectrometer consists of a laser light source, a complex set of optics, three photodiode arrays, processing electronics and a memory to store and read out particle size spectra (see optical system in Figure 11). The laser beam is focused onto an external prism supported about 15 cm from the pressure vessel's outer surface. The prism directs the beam back into the instrument where a set of lenses and beam splitters derive three independent optical trains. As a particle enters the instrument's field-of-view, its

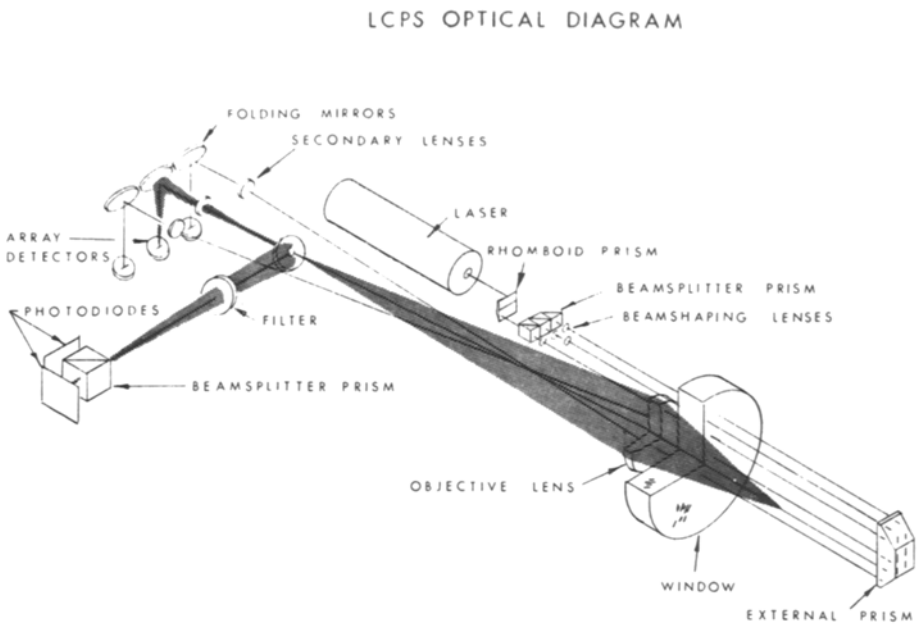

Fig. 11. (LCPS). LCPS optical diagram.

shadow is imaged onto a photodiode array. The shadow size is measured and recorded in the memory as a particle count of specific size. The particle size is simply related to the magnification and phodiode array element size.

The secondary LCPS sizing method involving the light scattered by single particles will use the same light beam as the 5–50 μm size range to extend resolution to sizes of 0.5 μm. This scattering subrange will have four size intervals of nonlinear weighting. A third measurement of particle transit time employed in conjunction with the 50–500 μm size range measurements will determine average particle 'thickness' when combined with descent velocity measurements. The ratio of particle thickness to measured size is the aspect ratio. The aspect ratio will help to distinguish particle morphology and differentiate crystalline particles from other spherical elements.

The LCPS requires a single optical penetration through the large probe pressure vessel wall. Additional structural penetrations are required to support the external prism. The instrument has two major subsections: (1) an internal instrument package housed within the pressure vessel and (2) an external prism assembly. The elongated laser tube and secondary imaging pathlengths dictate the internal instrument envelope depicted in Figure 12. The entire internal package is mounted rigidly to the large probe upper shelf which serves as the support structure for the experiment and it and the prism assembly are mechanically decoupled from the vessel wall by the use of flexible metallic bellows. The

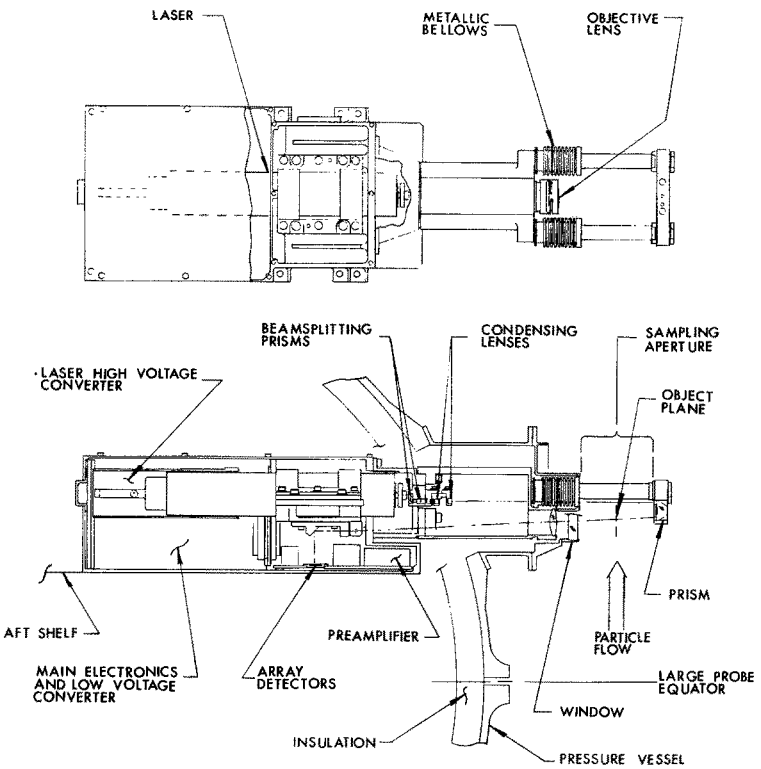

Fig. 12. (LCPS). Pioneer Venus LCPS instrument.

instrument has heated external optical surfaces and is capable of satisfactory operation over the expected environment. It can withstand contamination induced optical losses of more than 80%.

9. Large Probe/Small Probe Nephelometer (LN/SN)
B. Ragent/ARC and J. Blamont/CNES

9.1. Objectives

The Nephelometer experiments aboard the large and small probes will explore the vertical structure of the clouds of Venus, providing evidence for the existence or absence of particulates (solid or liquid) in the altitude region from about 67 km to the ground. Since it is expected that particles will be found to be distributed in layers, placing the instrument on all probes will help to determine whether the stratification is planetary in nature or varies from location to location. In addition,

the experiment will define the vertical extent and distribution of UV absorbers in the vicinity of probes descending in the sunlit side of the planet and also help to document the optical properties of the particulate distribution.

9.2. Concept and Approach

The method consists of illuminating the medium in the vicinity of the probe at distances outside of the aerodynamically disturbed atmosphere with a solid state light source operating at about 9000 Å and measuring the intensity of the light scattered by the particles of the medium in the backward direction (about 175°). Background solar scattered light will also be monitored in two wavelength intervals centered at approximately 3550 Å and 5200 Å, on the probes descending in the sunlit side with a vertical spatial resolution of less than 150 m.

The recorded nephelometer signals will yield the effective backward scattering functions of the clouds or hazes at about 9000 Å, as a function of altitude. The backward scattered signal is a measure of $N(\mathrm{d}\sigma/\mathrm{d}\Omega)$, where N is the particle concentration and $\mathrm{d}\sigma/\mathrm{d}\Omega$ is the differential scattering cross-section in the backward direction at a wavelength of 9000 Å. Until the probe reaches atmospheric depths where multiple scattering becomes appreciable, the background scattered light measurements may be used to derive values of $1/N\sigma_T$, the mean free path for light interaction, where σ_T is the total scattering cross-section of the particles at the appropriate wavelength. The difference between the values of mean free path at each wavelength is a measure of the amount of UV absorption at each altitude. Also, since each of the probes will be rotating, a crude angular scattering function for the particulate distribution may be obtained at the UV and visible wavelengths.

All of the above data, together with assumptions, for example concerning particle sphericity and refractive index, will be used to obtain fits to models of particle size distribution and particle density. Iterating these types of assumptions so as to obtain the best fit to the data will yield a set of particle sizes, refractive indices and particle densities for each altitude consistent with the observations.

9.3. Instrument Description

The instrument consists of an optical subsystem (OSS) and an electronic subsystem (ESS) that are integrated at a well-defined mechanical interface (Figure 13). The transmitted light beam, backscattered light beam and background solar scattered light pass through two windows mounted into the pressure shell of the probe. Calibration targets are affixed to the probe window covers for the small probe and the probe aeroshell in the case of the large probe, so as to allow for overall system calibration before the window cover or aeroshell is deployed after atmospheric entry.

9.3.1. *Optical Subsystem (OSS)*

The OSS consists of two major optical trains of elements comprising a transmitter and receiver system mounted on a bulkhead and two lens barrel assemblies. The

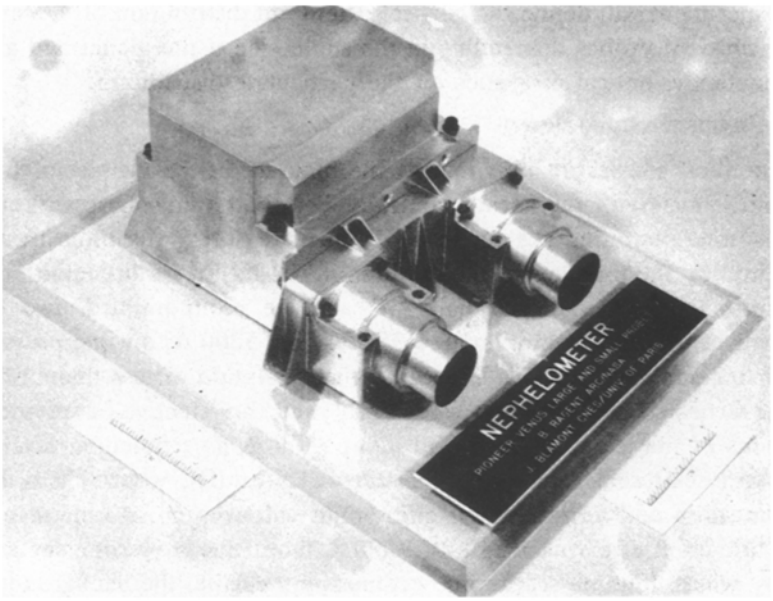

Fig. 13. (LN/SN). Pioneer Venus LN/SN instrument.

transmitter components consist of a solid state light emitting diode (LED), a plastic Fresnel lens for collecting and focusing the light and a set of two heat-absorbing borosilicate glass filters for thermal isolation of the lens and LED. A fiber-optics light pipe, shielded from direct reflections from other optical elements, is used to conduct a portion of the light reflected from the front surface of the spacecraft transmitter window to a detector in order to monitor the presence of deposits on the window and the condition of the transmitter LED. The receiver channel components include three solid state photodiodes for detecting the backscattered light, UV background and visible background, respectively, appropriate optical filter elements, a plastic Fresnel lens for focusing the backscattered light onto the backscatter detector, and two heat-absorbing borosilicate glass elements for thermal isolation. Additional thermal control and isolation and light collimation is provided by the lens barrels for each channel. The optical bulkhead also serves to mount and support components and to provide thermal paths for cooling critical elements. A monitoring and calibration system for detecting changes in the behavior of components is included in the OSS. This system consists of a separate calibration LED and fiber-optics light pipes to transmit calibration signals to all of the photodetectors. Finally, monitoring temperature sensors are mounted near critical components.

9.3.2. *Electronic Subsystem (ESS)*

The electronic subsystem contains all of the necessary components and circuitry to accomplish all of the required electronic functions of the instrument. These

include DC power conversion from the probe's bus supply to provide required instrument power, timing and logic control circuitry, conditioned LED pulse power, amplifiers, filters, multiplexers, synchronous detection boxcar integrators, digitizing equipment, data compression logic and telemetry interfacing circuitry. The ESS is housed in an enclosed roughly cubical compartment that mates with the OSS at the OSS bulkhead.

The digital data output from the ESS to the probe telemetry unit include primarily measurements of backscatter and UV and visible background. However, a number of calibration and monitoring data are also provided. These include transmitter window and LED monitor, calibration signals for all of the photodetectors, backscatter channel noise and DC offset, window monitor channel DC offset, transmitter LED temperature and a calibration flag signal. In addition, three housekeeping analog signals from two temperature sensors and a voltage reference level are made available to the telemetry unit for transmission.

9.3.3. *Instrument Performance and Physical Description*

Performance. The backscatter channel documents clouds having a value of $N(d\sigma/d\Omega) \simeq 10^{-5}$ to 10^{0} m^{-1} ster^{-1} (corresponding to a visibility from about 10 km to 10^{-4} km). Scattered solar background light is detected over a range of about 10^{-1} to $10^{10^{-5}}$ W m^{-2} ster^{-1} Å in both the UV and visible channels, each of which detects radiation over a spectral bandwidth of about 10^{3} Å. At the highest elevations of operation, backscatter data are sampled at least once per second and each background channel is sampled once every two seconds, corresponding respectively to a minimum resolution of about 100 m and 200 m at deployment, decreasing to less than 10 m at the planetary surface.

Physical description. The Nephelometer consists of a roughly cubical box with a sloping front panel (for clearance considerations) and with two protruding optical system barrels. The cube is roughly 8 cm on a side and the barrels protrude approximately 7 cm. The instrument is mounted on a shelf in either the large or small probe (somewhat differently for each probe), optical signals passing through the windows in the probe wall located about 3.5 cm beyond the end of the optical barrels. The instrument is encased in an aluminum case which serves to electrically isolate the instrument, mechanically support components and , most importantly, implement the thermal design necessary to keep the instrument within allowable temperature limits.

10. Large Probe/Small Probe Atmosphere Structure Experiments (LAS/SAS)
A. Seiff / ARC

The Comparative Atmosphere Structure Experiment (CAS) has temperature, pressure, and acceleration sensors on the Large Probe (LAS) and the three Small Probes (SAS). These instruments are used in a number of modes to measure or

determine upper atmosphere structure (200 to 65 km), lower atmosphere structure (65 km to impact), altitude above surface as a function of time, velocity as a function of time, trajectory path angle as a function of time, vertical flow velocities, atmospheric mean molecular weight, turbulent velocity fluctuation statistics, radial distance to the center of Venus, and seismic noise in the planet's crust if the probe(s) survive landing. Emphasis in measuring the atmospheric state properties is on achieving sufficient relative accuracy between probes to define the *differences* in thermal structure with entry location, and hence the thermal contrast which exists to drive the circulation.

10.1. Instrument descriptions

The temperature sensor, Figure 14, is a dual resistance thermometer, with one free wire element directly immersed in the atmosphere, for maximum sensitivity, response, and thermal coupling to the atmosphere, and one element bonded to the upper leg of the support frame, with adequate sensitivity, response, and thermal coupling, but higher survivability if unexpected hazards are encountered. The sensor is stimulated by a current source of 10 ma constant to within 20 ppm, and its potential drop is read through separate leads connecting to a high

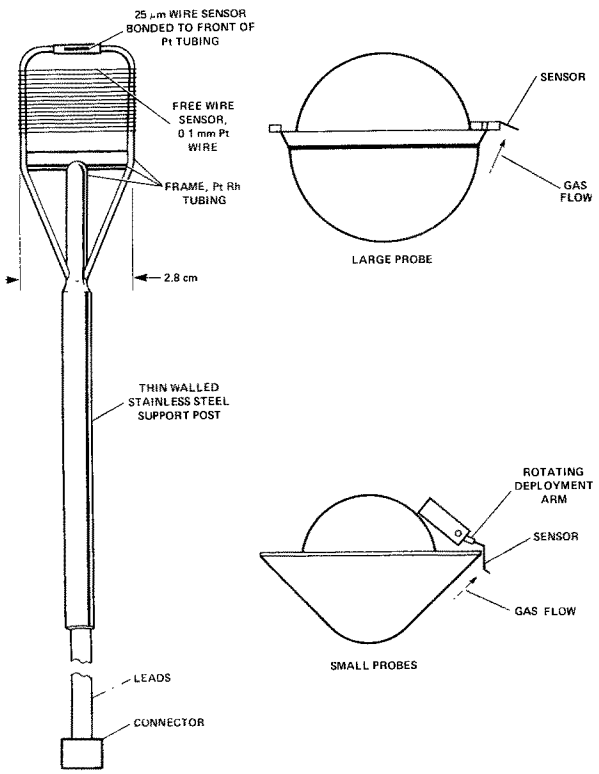

Fig. 14. (LAS/SAS). Schematic of the Pioneer Venus temperature sensor and its installation on the Probes.

impedance amplifier. The constant current source calibration is checked periodically during use by means of precision resistors switched in parallel with the sensor.

Extensive accuracy analyses of measurement errors due to conduction, planetary radiation, spacecraft radiation, thermal lag, self heating, electronic stability, flow velocity, mechanical strain, and thermoelectric emf have been performed, and each of these error sources has been limited by design choices to the level of about 0.1°C, maximum. (If each were 0.1°C, the RMS error for the nine error sources listed would be 0.3°C.) Errors tend to be largest at the highest altitudes, above 60 km, where thermal coupling to the atmosphere is the lowest, but the accuracy goal of 0.25°C will, it is believed, be realized or closely approached throughout the descent. The temperature measurement range is 200 to 800 K. The sensors are exposed to the atmosphere as shown in Figure 14, when the probes go below about 65 km.

The pressure sensors are multiple range, miniature, silicon diaphragm sensors. The wide dynamic range needed, from 30 mb to 100 bars (3300/1), is achieved by use of 12 sensors, each sized to measure over a pressure range of less than a factor of 2 ($2^{12} = 4096$). This geometric range selection permits nearly constant measuring accuracy (as percent of reading) over the full range. The sensing elements are nominally 3.2 mm in diameter by 1.6 mm long.

The 12 sensors are sampled in a way which also provides redundancy in case of loss or malfunction of any single sensor. They are divided into two sets, A and B. When a sensor in set A is primary, reading between 0.52 FS and FS (full scale), a back-up sensor in set B is read between 0.27FS and 0.52FS. When the set B sensor reaches 0.52FS, it becomes primary.

The sensor strain elements are diffusion bonded onto the pressure side of the diaphragm. Four resistors comprising a Wheatstone bridge are on the diaphragm, with two on the center, unsupported region of the diaphragm. These are the variable, opposite legs of the bridge. The other two resistors in the bridge are on the outer part of the diaphragm where they do not deform. The back side of the diaphragm is one end of a small reference chamber, which is sealed at vacuum during manufacture.

The 12 sensors are mounted in a housing designed to withstand 250 atmospheres internal pressure, and manifolded to the inlet port.

Our evaluation tests show that the sensors generally repeat output at a given pressure within 0.25% of full scale, short term, and the best of them, within 0.1%. The low pressure range units retain scale factor to within 0.5% over test periods of 6 months, while the higher pressure range units are even more stable. In dynamic thermal tests, at the expected temperature rate of 1°C min^{-1}, some deviation from equilibrium calibrations is seen on the lower ranges, but it is repeatable.

The acceleration sensors are derived from high accuracy guidance accelerometers. Acceleration is sensed by a pendulous mass, maintained in null position by

interaction of a current in a coil in the test mass with a permanent magnetic field. The nulling current is the measure of the acceleration. Deviations from null position are detected by symmetrical inductive sensing with a sensitivity of 1 μrad. The sensor body is approximately $3 \times 5 \times 5.3$ cm for each sensing axis. Four of these units comprise the Large Probe sensor (two sense the probe axial deceleration); one axial sensor only is on each of the Small Probes.

The sensors are range switched from 0.4 μg to 600 g by changing load resistors and amplifier gain, through four ranges during entry and two during terminal descent, to maintain high accuracy in each phase. Atmospheric sensing to about 200 km will be achieved. Sensor accuracy is expected to be better than 50 ppm on scale factor, with bias shifts less than 30 μg, in the presence of temperature changes during entry. This accuracy will permit velocity to be tracked to within about 2 m s^{-1} at worst, throughout the entry, but velocity changes in a sampling interval over most of the entry will be known to within about a cm s^{-1} in any single interval. Velocity tracking and measurements of g_{φ} post landing are the most critical requirements imposed. The latter will be sought to within 30 ppm, corresponding to an uncertainty in planetary radius of about 90 m.

The electronics package, which steps the experiment through four data formats, distributes power to all the above sensors, samples their outputs, changes their ranges, performs AD conversion to 8 or 12 bit resolution, and stores the data until the spacecraft calls for them, is in a box nominally $9 \times 9 \times 14$ cm. There are separate data formats for the high speed phase (termed Entry), the Descent phase, a transition phase between these two, and a landed (Seismic) phase. On the Large Probe, the experiment is assigned 74 bps in the high speed phase and allocates it entirely to the only measurement valid in this phase, acceleration. In the Descent phase, the experiment data allocation is 20 bps, of which 12 are assigned to p and T, 2 to defining aerodynamic deceleration and planet radius, 4 to statistics on atmospheric turbulence, and 2 to definition of probe angle of attack and aerodynamic asymmetry. The altitude resolution on pressure and temperature is 20 to 80 m, depending on probe descent speed. On the Small Probes, data allocations are 36 bps at high speed, used for deceleration measurements; 10 bps in the Descent phase above 30 km; and 4.75 bps in the Lower Descent. The latter permits pressure and temperature readings every 8 s, with altitude resolution of 150 to 64 m; and turbulence samples over 1.2 to 0.5 km altitude bands.

Turbulence sampling consists of counting the number of pulses in the sampling interval which exceed preselected acceleration levels, centered about the mean at 8 levels, 4 above and 4 below the mean. Seismic noise sampling is similarly implemented, with the fluctuating component of the landed acceleration due to gravity being monitored down to the 0.8 μg level.

11. Small Probe Net Flux Radiometer (SNFR) — V. Suomi/Wisc.

A Net Flux Radiometer (SNFR) instrument will be flown on each of the three small probes of the Pioneer Venus mission. The primary scientific goals are to

measure the net planar flux as a function of altitude and global position. The objectives of the measurement system are to cover the spectral bandpass of 0.2 to 50 μ, achieve a vertical resolution of 1 km, and to determine the net flux to an absolute accuracy of 2%. The instruments on each probe are identical and can operate equally well for either daylight or night time targeting.

The instrument consists of a Sensor Assembly (Figure 15) which is mounted outboard of the small probe pressure vessel and an Electronics Module mounted within the vessel. Immediately following the high 'g' deceleration and entry heating period, the sensor assembly is deployed from a protective enclosure to a position which locates the net flux detector beyond the turbulent boundary layer near the base of the probe heat shield. Data collection begins at about 72 km and continues until the end of the mission at surface impact.

The Sensor Assembly includes a net flux detector mounted on an extension shaft and an actuator which periodically rotates the detector and shaft 180 degrees. The periodic rotation is intended to both cancel instrument off-sets and to minimize errors caused by asymmetric heating of the detector. In addition to the flux plate, the detector includes a temperature sensor and a heater. The heater will minimize the possibility of condensing atmospheric constituents on the detector windows. It is turned on when the detector is deployed and remains on for the entire mission.

Two flux parameters are processed in parallel within the Electronics Module. These are a time averaged, or integral, flux, and the extreme values of a periodic input (maximum and minimum). Figure 16 illustrates the expected flux input to the detector for the probe targeted to the solar illuminated region. The input flux takes the noted waveform for two reasons. First of all the probe is spinning.

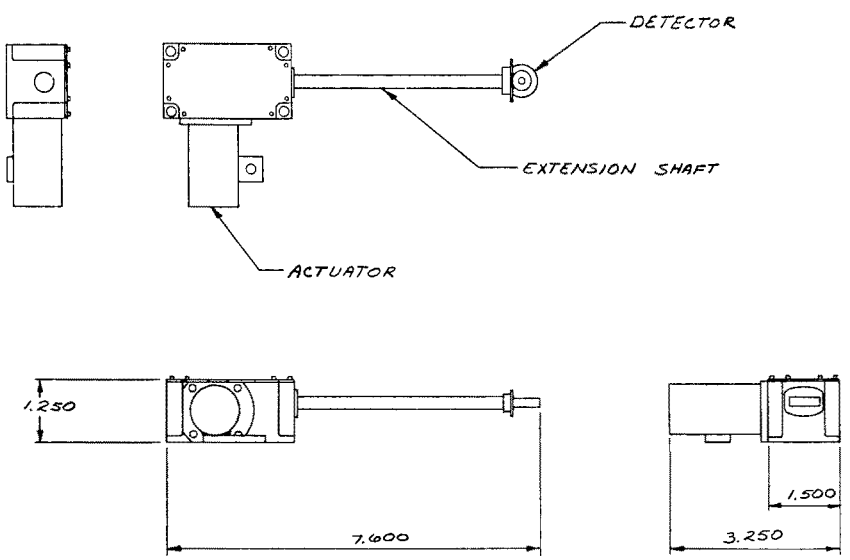

Fig. 15. (SNFR). SNFR sensor assembly.

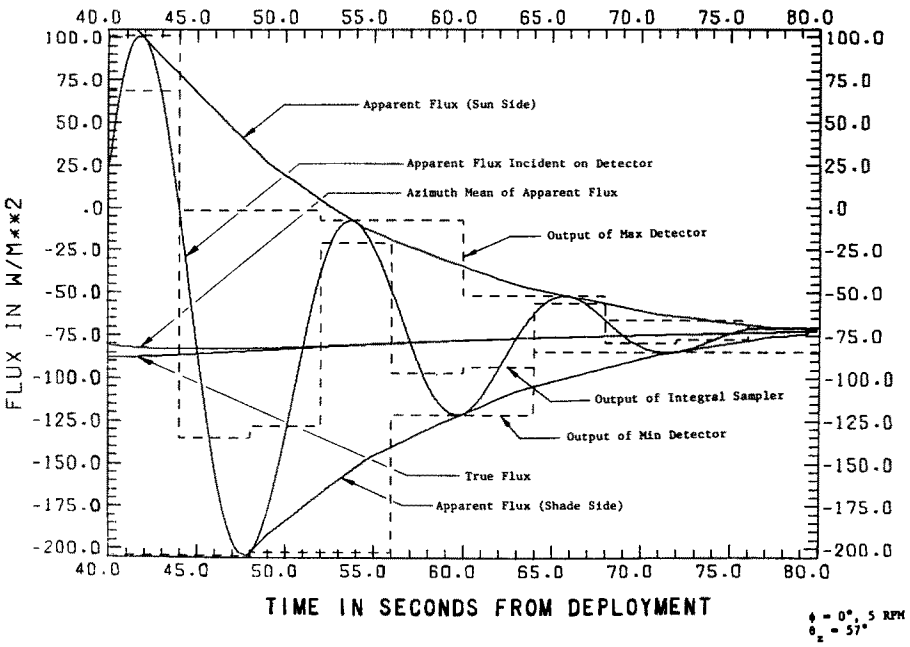

Fig. 16. (SNFR). Sensor input and output during descent.

Secondly, the detector does not see the direct solar beam through the full 360 degrees of rotation. Thus the amplitude of the modulation depends on the probe orientation relative to the Sun line, and the frequency depends on the probe spin rate. The three flux parameters which are measured are:

(1) The maximum value sampled over an 8 s window;
(2) The minimum value sampled over an 8 s window;
(3) The average value sampled over a 4 s window.

Figure 17 illustrates a simplified block diagram for the science data processor. The sensor output is amplified and is available to both the max/min and integral (average) data channels. The amplifier is chopper stabilized for low noise and low draft.

To determine the integral flux value, the amplifier output drives a voltage controlled oscillator (VCO) which in turn is fed into an Up/Down counter. The Up/Down counter is synchronized to the sensor position such that it counts up when the sensor is viewing 'Up' and counts down when the sensor is viewing 'Down' (i.e., rotated 180 degrees from the 'Up' position). It is important to keep in mind that the output voltage of the sensor reverses sign whenever the sensor is flipped.

The maximum and minimum amplifier voltage levels are sampled in overlapping eight second windows and held for readout into the probe telemetry stream. The output of the max/min detector is a gated frequency which is read into the

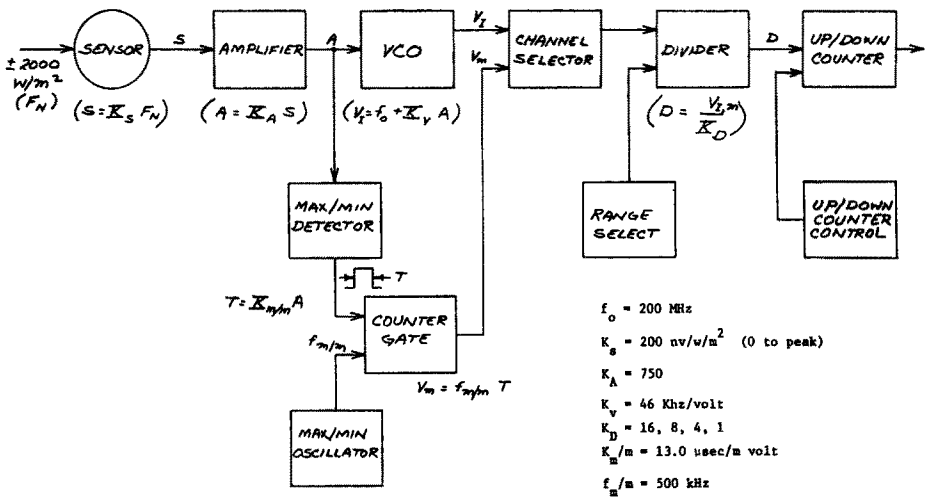

Fig. 17. (SNFR). SNFR science data processor functional block diagram.

Up/Down counter. For max/min samples, the Up/Down counter functions simply as a (unidirectional) counter.

The system operates over four dynamic ranges and is controlled by internal timing. The range change is implemented as a divider which serves both the integral and max/min systems.

In addition to the science data measurements described above, the instrument measures the detector housing temperature, and amplifier temperature as well as the status of the actuator, heater, and bit rate.

12. Differential Long Baseline Interferometry (DLBI)—C. Counselman/MIT

12.1. Introduction

Differential long baseline interferometry (DLBI) will be used to determine the velocity vectors of the four Venus probes, as functions of time, during the probes' descents through the atmosphere of Venus. These results, interpreted in terms of wind velocities, will be combined with the simultaneous measurements of atmospheric temperature, pressure, radiation-flux, and composition from other experiments in order to test models of Venus' atmospheric circulation (see Schubert *et al.*, this issue).

12.2. Method

While the four Pioneer probes are descending through the atmosphere of Venus, the 'bus' spacecraft will continue to follow a ballistic trajectory outside the atmosphere. The trajectory of the bus will be determined by conventional two-way Doppler tracking techniques, with the uncertainty in the bus' velocity

with respect to Venus expected to be less than 10 cm s^{-1} in all 3 vector components. Two-way Doppler tracking of the large probe, and one-way tracking of the 3 small probes, should also enable the component along the line of sight (from Earth to Venus) of each probe's velocity vector to be determined with an uncertainty no greater than 30 cm s^{-1}. To determine the remaining two components of each probe's velocity vector, normal to the line of sight, I. I. Shapiro suggested that the new technique of DLBI (Counselman *et al.*, 1972, 1973) be used.

The DLBI technique requires at least three widely separated stations on Earth to receive, simultaneously, the S-band radio signals emitted by the probe and the bus spacecraft. The difference between the phases of the signals received at two stations from a given spacecraft is sensitive to motion of the spacecraft normal to the Earth–Venus line of sight and in the plane containing the spacecraft and those two stations. A third, non-coplanar receiving station is needed to determine the third component of the spacecraft's velocity vector. For reliability a total of 4 stations will be used in the Pioneer Venus experiment: the 64 m Deep Space Stations at Goldstone, California, and Canberra, Australia, and the 9 m Spaceflight Tracking and Data Network Stations at Gaum and at Santiago, Chile.

The interferometric phase observable which is formed by the between-stations differencing is insensitive to any variations in the phase of the signal emitted by the spacecraft, and to the effects of the propagation medium near the spacecraft. Another differencing, between the interferometric observables obtained simultaneously for the bus and for one of the probes, yields the DLBI observable, which is sensitive to the motion of the probe relative to the bus, but is insensitive to errors associated with the receiving stations and with the atmosphere above these stations. (See Figure 18.) Thus, for the DLBI determination of the probes' motions in Venus' atmosphere we will rely on the accurate determination, by two-way Doppler tracking, of the ballistic trajectory of the bus. The bus will be our 'benchmark'.

12.3. Expected uncertainties

What are the uncertainties of the results of the Pioneer Venus DLBI experiment likely to be? A detailed error analysis (Pettengill *et al.*, 1975), supported by the extensive results available from other DLBI experiments (Counselman *et al.* 1972, 1973; King, 1975; Counselman, 1976), indicates that all components of the probes' velocity vectors relative to Venus, after averaging over time intervals of 2 min, will be determined with uncertainties smaller than 50 cm s^{-1}. The dominant source of error is expected to be receiving-system 'background' noise at the smaller (9 m diameter antenna) receiving stations. Time resolution of 2 min corresponds to altitude resolution of the order of 10% for altitudes above about 10 km, and to ~1 km resolution below 10 km, for both the large and the small probes. Altitude- or time-resolution may also be traded for velocity–measurement

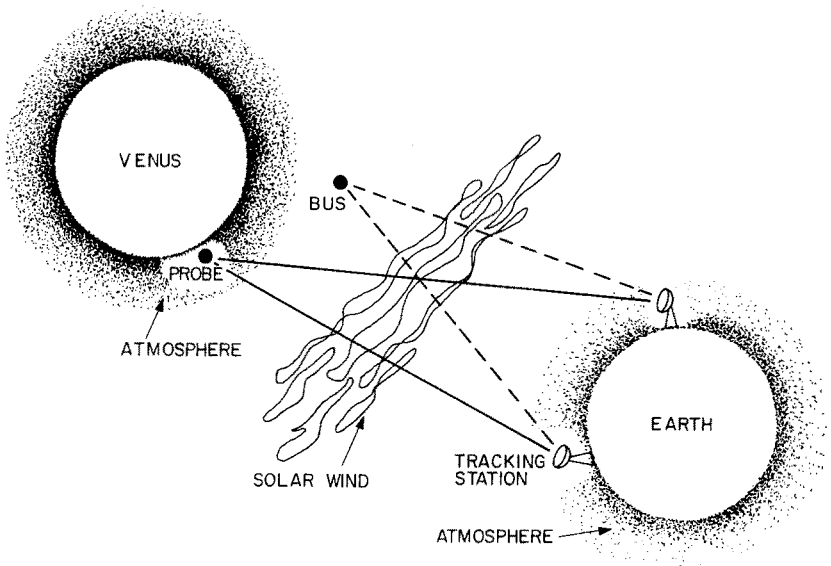

Fig. 18. (DLBI). Sketch of the geometry of the DLBI observations, with the atmospheric and the interplanetary propagation media indicated. Because the propagation paths are so nearly parallel, and because the DLBI observable is differenced symmetrically with respect to both the transmitting spacecraft and the receiving ground stations, the effects on the observable of both Venus' and the Earth's atmospheres cancel to a high degree. The interplanetary plasma is not a major error source, although its effects are not cancelled so exactly by the observing geometry.

accuracy: The velocity uncertainty is approximately proportional to $t^{-1.5}$, where t is the averaging time.

13. Wind Speeds in the Venus Atmosphere From Doppler Tracking of Probes (MWIN)—A. Kliore/JPL

As the probes descend through the atmosphere of Venus, the Doppler frequencies of the telemetry signals will be recorded and analyzed to estimate winds in the atmosphere of Venus along the Earth-probe line-of-sight. These data will be complimentary to the results obtained from the DLBI experiment.

The descent trajectory for each probe will be estimated from a combination of radio tracking, atmospheric density profile, and aerodynamic model of the probe. The atmospheric density profiles will be obtained from the *in situ* observations by the probes. For entry locations well away from the sub-earth point, the primary result will be the horizontal component of the wind, while vertical wind velocities will be measured for entry locations near the sub-Earth point.

14. Atmospheric Propagation Experiments (MPRO)—T. Croft/SRI

The probes send their information back directly to Earth at S-band, 2300 MHz. Some information about the local environment may be gleaned from the effects of that environment on these signals. During the descent of each probe in the

atmosphere, a careful search will be made for evidence of the signal which travels downward, reflects off the surface of Venus and then propagates to Earth. This will be Doppler shifted away from the direct signal by less than 1 kHz and is expected to be very weak. A successful detection would yield information on the structure of the Venusian surface and also on the large-scale vertical profile of the terrain. The probe antennas have not yet been evaluated in the direction of the ground-reflected signal and so the strength of the signal cannot be predicted with confidence.

14.1. Atmospheric and ionospheric scintillation

Turbulence in the atmosphere or ionosphere causes inhomogeneity in the refractive index with the result that passing radio signals scintillate. The probe–orbiter combination promises to yield an excellent body of observations for the study of this phenomenon, resulting in a great increase in our information about the underlying turbulence. The probe signals will pass through the medium at an incidence angle about 60° from the vertical, while the orbiter signals will make their transit essentially in the horizontal direction. Anisotropy in the turbulence should lead to a difference between the characteristics of the resulting scintillations. From this, the anisotropy can be evaluated. Vertical inhomogeneity will be revealed both by the probes and by the orbiter, although the latter will work only down to heights of some 35–40 km due to the super-refraction limit. Inhomogeneity in latitude and longitude may be revealed by the orbiter, since it can provide independent occultations at as many as 160 places on the globe (see 28 OGPE). If one or more of the probes survives a few seconds after landing in an orientation that allows signal transmission to Earth, then the character of the scintillation should change because the probe will no longer be moving behind the turbulent medium. This will permit a determination of the relative importance of temporal and spatial inhomogeneity in the atmosphere.

The strength of the signals from the probes will diminish during descent because of three aspects of propagation: first, there will be a loss due to defocussing by the action of refraction in the atmosphere. Second, there will be some absorption of the signal by the CO_2 which forms the bulk of the atmosphere. Third, there is expected to be additional absorption due to stratified layers of clouds or other absorbing material. Each of these three losses will increase during the descent; each is greater if one increases the distance from the sub-Earth point, due to the more oblique path in the atmosphere. The strength of the probe signals will be measured primarily as a means of identifying the third listed absorption; if this is due to a cloud layer, the height and thickness of the layer may be determined.

15. Atmospheric Turbulence Experiment (MTUR)—R. Woo/JPL

Measurements of the variation of the intensity of turbulence with altitude and

solar zenith angle, wind velocity transverse to the line-of sight path and the distribution of turbulence scale sizes in the atmosphere of Venus will be made using the S-band radio scintillations observed during atmospheric entry. The procedure consists of two steps: (1) processing of digitized radio signals during atmospheric entry and (2) theoretical analysis of wave propagation in a turbulent medium. Turbulence information is then obtained by comparing steps (1) and (2). Data analysis is based on the variances and temporal frequency spectra of the amplitude and phase scintillations.

16. Orbiter Neutral Mass Spectrometer (ONMS)—H. Neimann/GSFC

Mass spectrometry is employed to measure the number densities of the neutral particles in the upper atmosphere of Venus in an altitude range from approximately 150 km (perigee) to 500 km.

A quadrupole mass spectrometer with an electron impact ion source and a secondary electron multiplier ion detector will be used. The ion source is designed to be operated alternately in a 'closed source' and an 'open source' mode. The closed source mode allows accurate concentration measurements of noble gases and of some non-reactive gases, for example, CO_2 and N_2, and the open source configuration allows a concentration measurement of chemically active gases. A schematic diagram of the mass spectrometer is shown in Figure 19.

In the open source mode only ions produced in the ionization region resulting from free streaming particles are analyzed by the mass spectrometer. Taking

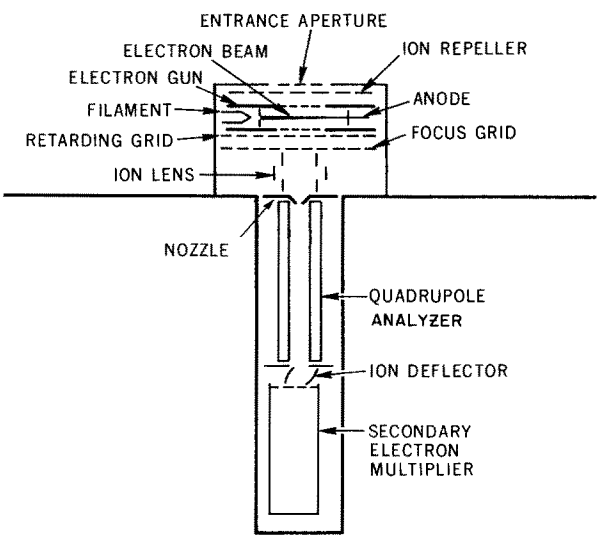

Fig. 19. (ONMS). Pioneer Venus Orbiter Neutral Mass Spectrometer.

advantage of the large relative kinetic energy of the free streaming particles with respect to the orbiter, a retarding potential principle is used to discriminate between the surface reflected and the free streaming particles after ionization by the electron beam, when the instrument axis points in the general direction of the velocity vector.

In the closed source mode both free streaming and surface reflected particles are analyzed after ionization. The source is located inside the chamber which is connected to the ambient atmosphere via a knife-edge orifice, allowing the surface reflected particles to accommodate to the surface temperature before ionization.

To discriminate between constituents of equal atomic mass, for example CO and N_2, and to reduce the excess kinetic energy of dissociatively ionized species, the kinetic energy of the electrons can be chosen by ground command to be either 90 or 27 eV.

The quadrupole analyzer consists of hyperbolically contoured rods 7.5 cm long with a field radius of 0.2 cm. The mass peaks produced by the rod assembly have flat tops which permit stepping from mass unit to mass unit without requiring peak searching. Specific masses are selected by stepping the applied AC and DC voltages. The ions exiting the analyzer will be deflected into the entrance aperture of a secondary electron multiplier which effects charge conversion and amplification. The charge pulses at the multiplier anode are counted by a pulse detector, and the current is measured by an electrometer amplifier to extend the dynamic range of the instrument. The counting rate and the electrometer current are proportional to the particle density in the ionization region of the ion source.

The mass spectrometer is bakeable to 350°C for vacuum clean-up and will be maintained below 10^{-6} torr pressure during launch preparations and cruise. A small getter pump is provided as part of the mass spectrometer housing to maintain a low pressure after sealing. A pyrotechnically actuated break-off device will expose the ion source to the ambient atmosphere approximately 2 days after orbit insertion. The instrument is mounted on the orbiter instrument platform with its axis 27° from the spin axis. This allows the minimum angle of attack to be equal or smaller than 15° during a periapsis pass, and the maximum angle of attack less than 80° during a spin period.

The mass spectrometer can be programmed by ground command to scan continuously from 1 to 46 AMU or to scan any combination of masses within this range. Open source, closed source or flip-flop operation can also be chosen by ground command. Because of the limited data rate available, the sampling will occur either equally spaced in time over a spin period or be restricted to approximately ±45° of the spin angle around the ram position of the instrument axis.

The maximum average vertical spacing of the sample points is approximately 400 m at 500 km altitude and the horizontal spacing along the satellite path is approximately 2 km. Table VII summarizes pertinent instrument parameters.

TABLE VII
Instrument parameter summary

Mass Analyzer	:	Quadrupole
Ion Source	:	Neutral particle retarding potential/enclosed (ground programmable)
Ion Detector	:	Secondary Electron Multiplier (pulse counting/electrometer)
Mass Range	:	1 AMU to 46 AMU
Density Range	:	(1) 1×10^{5} cm^{-3} to 2.5×10^{12} cm^{-3} ion source density (2) 5×10^{3} cm^{-3} to 2.5×10^{12} cm^{-3} ambient density
Resolution/Crosstalk	:	$<10^{-4}$ for adjacent mass
Sampling Rate	:	6 samples s^{-1} nominal 56 samples s^{-1} maximum (±45° forward looking) 14 samples s^{-1} average (equal time spacing)
Dimension/Shape	:	Cylinder, 16 cm diameter 31 cm total length (including breakoff cap) 26 cm length electronics package
Ion Source Deployment Mechanism	:	Metal–ceramic breakoff cap, pyrotechnically actuated

17. Orbiter Retarding Potential Analyzer (ORPA)—W. Knudsen/LPARL

The Orbiter Retarding Potential Analyzer (ORPA) will measure several important plasma quantities in the ionosphere, planetary tail, and boundary layers surrounding Venus. Figure 20 illustrates two trajectories of the orbiter through these regions, one when periapsis is near local noon and one near local midnight. The ORPA axis is offset from the spacecraft spin axis, to permit close alignment of the ORPA axis with the orbiter velocity vector during a portion of each spin cycle near periapsis.

The quantities measured by the ORPA and their spatial resolutions, ranges and uncertainties are listed in Table VIII. The measurement of ion composition and temperature (or four electron temperatures) at intervals along the trajectory of approximately 120 km is achieved by on-board analysis and selection of the most significant portion, or portions, of one retarding potential scan in each spin revolution. Each scan, is completed in a small fraction of a spin period. Scans are taken repeatedly and that scan for which the instrument is optimally oriented is sensed, stored, and transmitted to Earth. Thus a spatial resolution of 120 km is achieved with the small bit rate assigned to the ORPA. Although a spatial resolution of 120 km for ion temperature measurement is coarse by Earth satellite standards, this resolution will provide approximately fifty measurements along that portion of the trajectory lying below the ionopause on the day side (Figure 20). The vector ion velocity is measured by recording three ion scans recorded at three different instrument celestial longitudes, in three successive spin cycles. In a special mode, the total ion concentration can be measured at 20 m intervals.

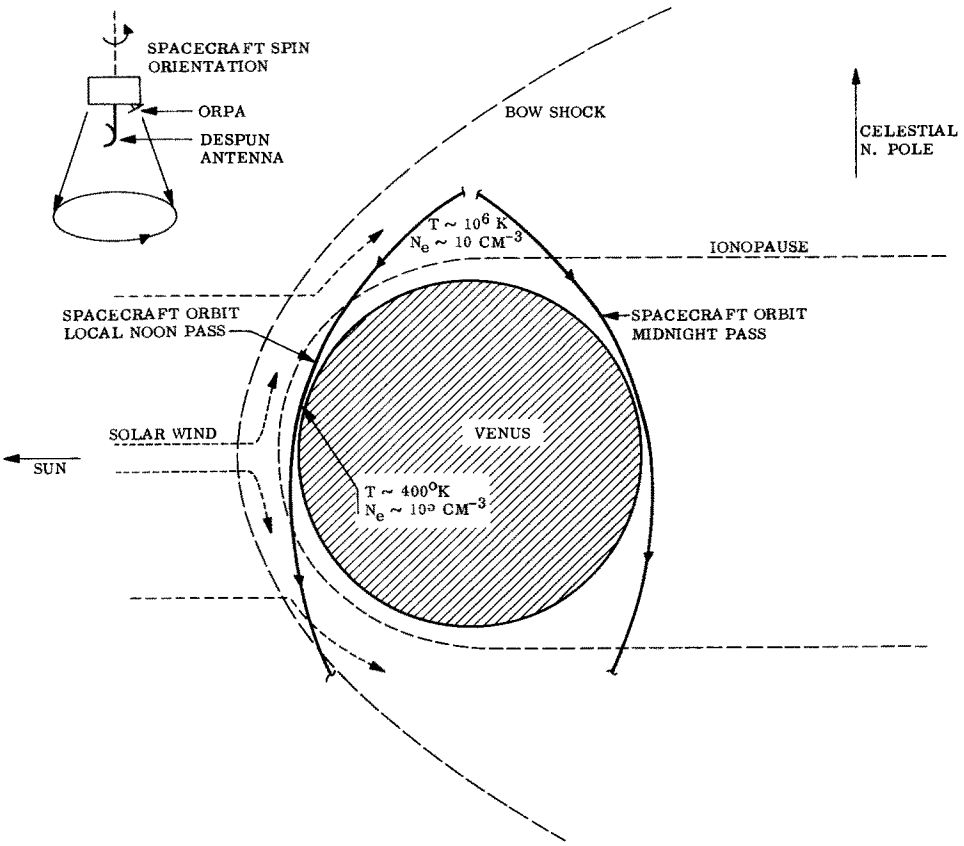

Fig. 20. (ORPA). Trajectory of the Orbiter spacecraft through the Venusian plasma regions. Spacecraft and ORPA orientation are also illustrated.

The ORPA, shown schematically in Figure 21, is a modification of the West German AEROS RPA (Spenner and Dumbs, 1974). Large-area entrance grids and collector guard ring provide a uniform flux radially from the instrument axis. The collector samples the uniform, central flux region. Systematic error is minimized by use of multiple retarding grids coated with colloidal graphite. A 30 cm diameter ground plane surrounds the entrance grid G_0 and provides for a planar plasma sheath even at low electron concentration.

The ORPA is operated in an electron Langmuir probe mode, *E*, an ion mode, *I*, and a photoelectron mode, *P*, by application of the control voltages and retarding potential staircase programs specified in Figure 21.

The staircase program is linear in the *E* mode and quadratic in the *I* and *P* modes for optimum sampling of the *I–V* curves. Control voltages are applied in each mode to suppress either electrons or ions as appropriate. Theory of operation of the RPA in the ion mode is described by Knudsen (1966).

TABLE VIII
Measured plasma quantities

Symbol	Quantity	Sample distance[a]	Closest distance between samples[b]	Range[c]	Uncertainty[d]
$N_i\ (=N_e)$	Total ion concentration	1 m	20 m	~ 10–$10^7\ cm^{-3}$	~5%
N_i^j	Concentrations of up to four abundant ions	1.6 km	120 km	$\sim 10^2$–$10^7\ cm^{-3}$	~5%
T_i^j	Temperature of the jth ion	1.6 km	120 km	300–10 000 K, $\sim 10^2 < N_i < 10^7\ cm^{-3}$	~5%
M_i^j	Mass of the jth ion	1.6 km	120 km	1–56 AMU	~1 AMU
$\bar{D}$	Ion drift velocity	1.6 km, 240 km	500 km	0.05–5 km s^{-1}	~50 m s^{-1}
f_e	Low-energy electron distribution function	0.5 km	120 km	0–60 eV, $\sim 10^6$–10^{12} $cm^{-2}\ s^{-1}\ ster^{-1}\ eV^{-1}$	~20%
T_e	Electron temperature	0.4 km	0.4 km, 120 km	300–20 000 K, $\sim 10^2 \leq N_e \leqq 10^7\ cm^{-3}$	~10%

[a] This is the distance traveled by the spacecraft at a velocity of 10 km s^{-1} during which the plasma is sampled.
[b] This distance is dictated by assigned bit rate.
[c] These ranges depend in some instances on the values of other parameters such as ion composition.
[d] These uncertainties apply to the higher concentration ranges. As the concentration drops toward $10^2\ cm^{-3}$, the accuracies will degrade.

To achieve the spatial resolution indicated in Table VIII for the E and I modes, it is necessary to transmit to earth only selected data from the resulting I–V curve. Selection is achieved by on-board recognition of points of inflection of the I–V curve in regions of negative dI/dV. Appropriate data about the inflection point are selected for transmittal. As an example, the numerically simulated response of the ORPA in the ion mode is illustrated in Figure 22. The current steps correspond to the quadratically varying ion retarding potential step generator. First and second differences of I_i are formed in this mode and used to recognize the peaks in ΔI_i corresponding to the more abundant ion species. Four ions expected in the Venusian ionosphere, all of equal concentration and temperature, were used in the simulation. A maximum of four sets of five values of ΔI_i, each spaced around a peak in ΔI_i, are selected together with I_i^1 and I_i^{80} for transmittal. Concentrations and temperatures of the selected ion constituents are determined by least squares fitting of the theoretical expression for the finite differences of ΔI_i to the observed values.

In addition to the 'peak select' mode of operation, the ORPA may be commanded into an I–V mode of operation in which every other value of I_e in the electron mode and I_i in the ion mode are stored for transmission. In this mode, the I–V curve is transmitted every third spacecraft revolution. This mode is expected to be useful in verifying the correct analysis of the results obtained in the 'peak select' modes of operation.

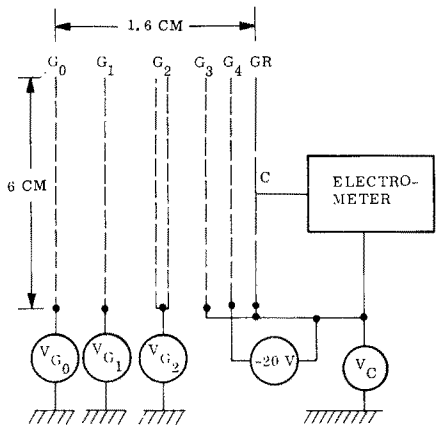

CONTROL VOLTAGES†

SYMBOL	ELEMENT	ELECTRON MODE	ION MODE	PHOTOELECTRON MODE
G_0	ENTRANCE GRID	7.8 → -4.8	0 OR -4.8	0
G_1	ION SUPPRESSOR GRID	7.8 → -4.8	-0.5* → 39*	47
G_2	ION RETARDING GRID	7.8 → -4.8	-0.5* → 39*	0 → -60
G_3	DISPLACEMENT CURRENT SHIELD	47	-4.8	47
G_4	ELECTRON SUPPRESSOR GRID	27	-24.8	27
C.GR	COLLECTOR. GUARD RING	47	-4.8	47

STAIRCASE PROGRAM†

MODE(S)	SCAN	NUMBER STEPS	STEP SIZE (VOLTS)	VOLTAGE RANGE (VOLTS)
E	ELECTRON COARSE	64	-0.2	7.8 → -4.8
	ELECTRON FINE	20	-0.05**	1.0**
I	ION	80	J × 0.0125 V J = 1.80	-0.5* → +39*
P	PHOTOELECTRON	25	J × 0.2 J = 1.25	0 → -60

† Referenced to satellite ground except those starred.
*Referenced to plasma potential.
**Subdivides five coarse steps.

Fig. 21 (ORPA). Sensor schematic and control voltage programs.

The ORPA is being supported by NASA and the Federal Republic of Germany.

18. Orbiter Electron Temperature Probe (OETP)—L. Brace/GSFC

18.1. Objectives

The primary purpose of the Orbiter Electron Temperature Probe (OETP) is to provide measurements of the electron thermal structure of the Venus ionosphere

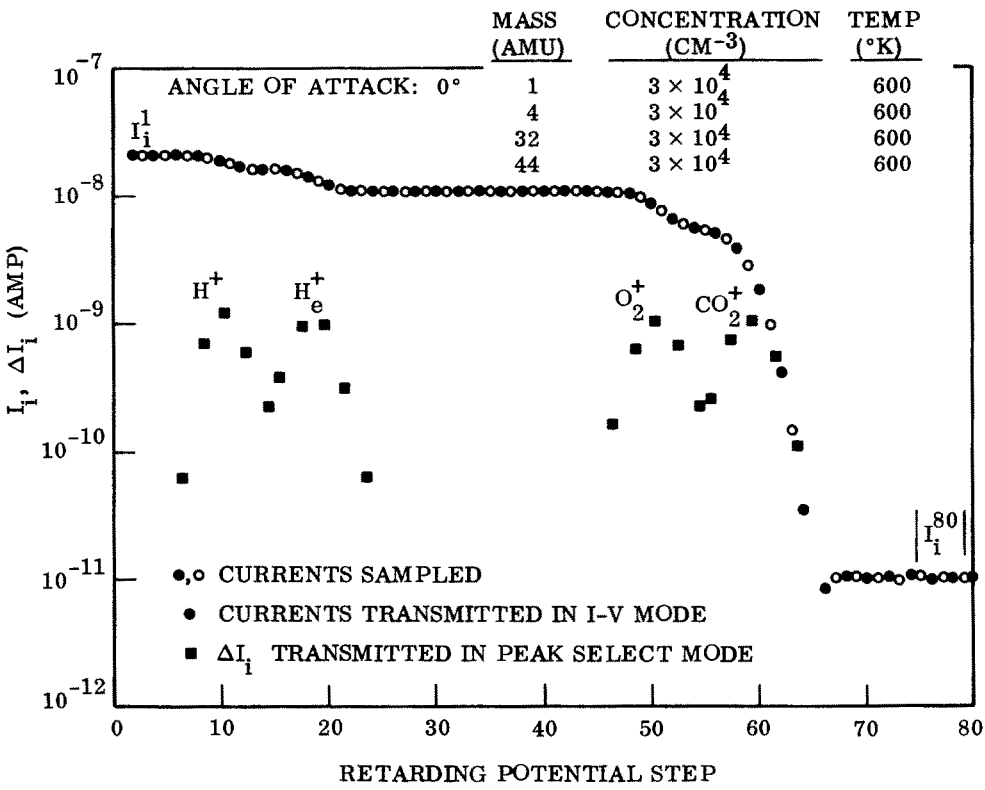

Fig. 22. (ORPA). Numerical simulation of an ion characteristic. Instrument operation and data selection are illustrated.

and its variations with time and location. These data will permit us to better understand the processes by which the ionosphere is heated and cooled. The instrument measures the electron temperature, T_e, the electron concentration, N_e, ion concentration, N_i, and spacecraft potential relative to the plasma, V_s.

18.2. The method

The OETP employs two cylindrical Langmuir probes of a design similar to that used on Atmosphere Explorer spacecraft by Brace *et al.* (1973). Figure 23 shows the mounting locations of the sensors on the orbiter. Each collector is 76 mm long and 2.0 mm in diameter. The axial sensor is mounted parallel to the spacecraft spin axis and is placed on a boom 0.4 m long. The radial sensor is mounted radially on a boom that is 1.0 m long. The function of the booms is to place the collectors as far from the spacecraft as is feasible to reduce errors introduced by spacecraft photo emission and the spacecraft ion sheath that become important at very low electron concentrations.

The theory of OETP operation is illustrated in Figure 24 which shows schematically the form of the current-voltage characteristic of a Langmuir probe in a

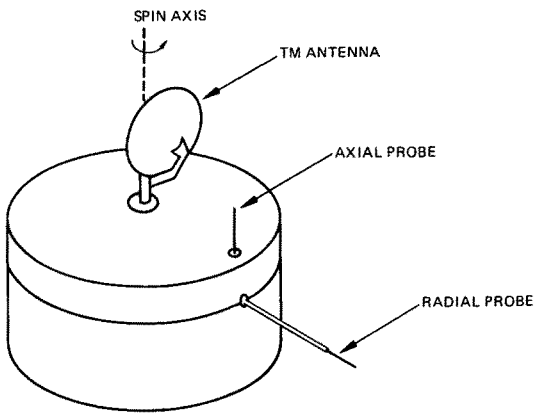

Fig. 23. (OETP). Mounting arrangement of the two Langmuir probes. The axial probe is mounted on a boom 0.4 m long, while the radial probe employs a 1.0 m boom.

plasma. N_i is derived from the ion saturation current, I_i, using the expression given by Hoegy and Wharton (1973). The value of T_e is derived from the exponential rise of the electron current, I_e, in the retardation region. The value of N_e is derived from the saturated electron current (Spencer *et al.*, 1965). The electron current is measured from a linear extrapolation (shown dashed) of the ion saturation region.

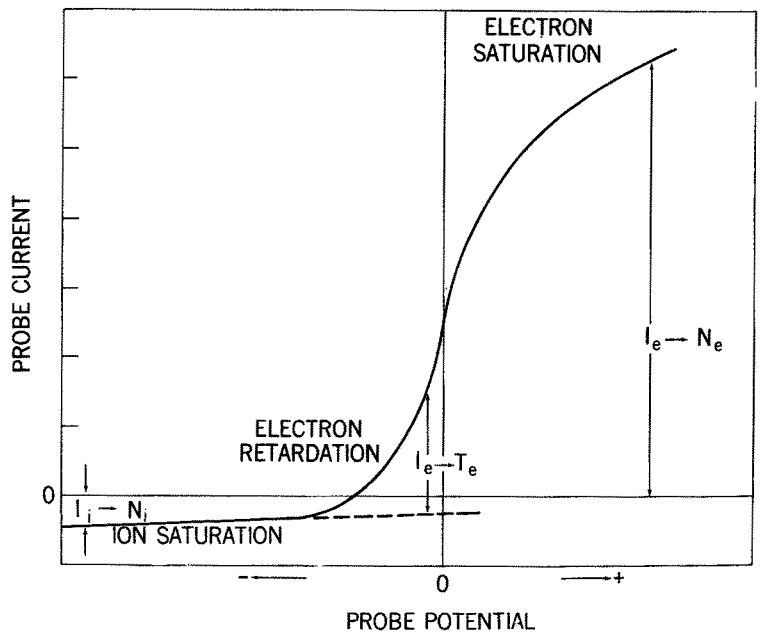

Fig. 24. (OETP). Current–voltage characteristic of a Langmuir probe showing the regions from which N_i, T_e and N_e are derived.

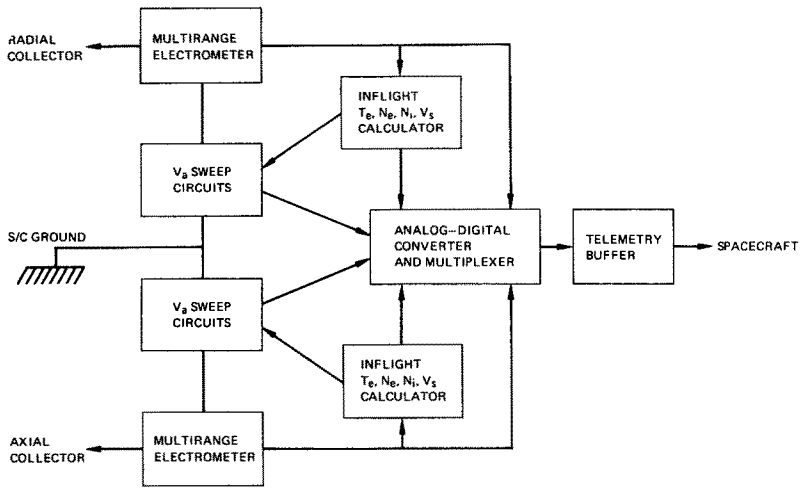

Fig. 25. (OETP) Electronic unit for the OETP. Independent electrometer and sweep circuits service the two probes. Inflight analysis circuitry adapts the sweep voltages and electrometer gains to match the existing plasma conditions. Occasional full volt ampere curves are stored and telemetered for ground verification of the inflight analysis.

18.3. The Electronics

Each probe is operated independently by its own sweep voltage generator and electrometer, although they share other functions provided by the electronics as shown in Figure 25. Each probe is swept twice per second with a sawtooth voltage whose amplitude and bias level are controlled adaptively by the in-flight analysis circuitry. These circuits automatically adjust the electrometer gain and match the sweep amplitude to the electron density and temperature currently being measured, (Brace *et al.*, 1973). The sweep amplitude will be varied automatically over the range of 0.5 to 10 V depending upon the electron temperature that is currently being measured. The same adaptive circuitry will also introduce a suitable bias voltage to compensate for changes in spacecraft potential up to ±5 V. Automatic current ranging circuits will sample the ion current at the beginning of each sweep and will adjust the electrometer gain to a value commensurate with the variations in ion concentration. These adaptive functions are designed to optimize the resolution of volt–ampere curve over the widest possible range of N_e and T_e. As a check upon the inflight analysis, approximately one curve per spacecraft spin period (12 s) is sampled at 50 equally spaced voltages. These points are telemetered for ground verification of the onboard analysis.

18.4. Measurements Provided

As noted earlier, the instrument measures T_e, N_e, N_i and V_s. The spatial resolution in these measurements depends upon the data rate currently employed

by the spacecraft. In modes in which both probes are being used the maximum data rate permits four values of T_e, one N_e and N_i each second, and one V_s every two seconds. As a result of satellite spin the two probes will not always be in position to obtain valid measurements. The effective resolution may then be reduced to one or two measurements per spin period.

A commandable mode is available which permits the above sampling rates to be dedicated to either one of the two probes rather than alternating between probes. For example, where N_e is found to be very low, the full data rate can be dedicated to the radial probe whose long boom should make it less susceptible to errors at low N_e. Conversely, at low altitudes where N_e is higher, the system can be dedicated to the axial probe whose mounting location will make it relatively free of spin modulation, thus improving the spatial resolution that can be obtained.

18.5. Accuracy

The accuracy of the measurements will vary with the specific plasma conditions, but nominal errors in T_e and N_e should be less than 10% where ever N_e exceeds 10^3 cm^{-3}. The accuracy will decrease at low concentrations because of the sheath and photoelectron emission effects noted earlier. We may be able to measure T_e at densities as low as 10^2 cm^{-3}, but this will depend upon factors of spacecraft design that cannot be evaluated fully at this time.

Because of photo emission from the collectors themselves, which is an apparent ion current, when the spacecraft is in sunlight N_i will be measured accurately only when it exceeds about 5×10^3 cm^{-3}. The N_e measurements will be limited by photo electrons reaching the collector from the spacecraft surface. When the radial probe is on the dark side of the spacecraft the photoelectron currents will be reduced and it may be possible to measure N_e as low as 10 cm^{-3} (Brace *et al.*, 1971).

19. Orbiter Magnetometer (OMAG)—C. Russell/UCLA

The objectives of the magnetic fields investigation on the Pioneer Venus Orbiter revolve principally around the study of planetary magnetism and the study of the interaction of the solar wind with the planet. The study of planetary magnetism includes the measurement of the magnetic dipole and higher multipole moments and the search for surface correlated magnetic features such as those due to regions of crustal remanent magnetization, magnetized perhaps in some earlier epoch when the planetary field was stronger. The measurement of the planetary dipole moment of our sister planet, so similar in size to the Earth yet so different in its rotation rate, will provide a key data point in the quest to unlock the mystery of the planetary dynamo mechanism. We have known the magnetic moment of the Earth for over three centuries but cannot say what fluid motions give rise to this field, nor what energy source drives those fluid motions.

The study of the solar wind interaction with the planet includes determining whether the planetary magnetic field, an induced magnetic field, or the ionosphere itself deflects the solar wind around the planetary obstacle, or whether it is a combination of these processes. The question of the effect of the pick up of ions by the solar wind due to charge-exchange with and photoionization of the Venus geocorona both on the solar wind and on the structure of the upper atmosphere will be studied, as will the connectivity of the ionopause to the solar wind. Is it effectively shielded from the mass, momentum and energy flux of the solar wind, or does a significant fraction of the solar wind penetrate the ionosphere? Our experience with the terrestrial magnetosphere and ionosphere may be of little help here.

19.1. The instrument

The magnetic field instrument is a fluxgate magnetometer, with sensors mounted on long booms to isolate them from the magnetic fields of the spacecraft and subsystems. The electronic design closely follows that of the ISEE-A and B fluxgate magnetometers due to be launched in 1977 which in turn evolved from designs used on the ATS-1, ATS-6 and OGO-5 spacecraft. The magnetometer consists of three ring core sensors on a 6 m boom together with an electronics unit on the main body of the spacecraft. The use of a long boom permits the measurements of magnetic fields as small as nanoteslas on a spacecraft with a rather high magnetic moment, of the order of 1 mA m^{-2}. Two of the three sensors are mounted at the end of the boom: one parallel to the spin axis and one perpendicular to the spin axis. The third sensor is mounted one-third the way down the boom from the other two sensors and tilted at a 45° angle to the spin axis. In quiet magnetic fields, either the two outer sensors, or the inner sensor alone provides sufficient information to reconstruct the three vector components of the magnetic field. This in turn permits a measurement of the gradient of the spacecraft magnetic field. Examination of this gradient as a function of time permits a valuable check on the stability of the spacecraft field.

The sensors consist of a metal ring around which is wound a ribbon of a highly permeable alloy. This core is then wrapped with a set of drive, sense and feedback coils. The drive coils force the permeable metal into saturation at a frequency of 7.25 kHz. External fields along the sense axis of the ring core cause it to enter saturation asymmetrically producing a signal at the second harmonic of the drive frequency. A feedback signal proportional to the strength of the second harmonic is applied to the feedback coils to null out the external field so that the basic magnetometer always operates in or near a zero field condition. The strength of the feedback signal is then a measure of the component of the external field along the sense axis of the ring core sensor. After detection the signals pass into the data handling assembly. Here the feedback current is digitized to 12 bit accuracy for each of the three sensors. These 36 bits are compressed into one 32 bit word by conversion to floating point words, thus removing the need for gain changes

when the instrument moves from a low to a high field region and vice versa. The range of the instrument remains fixed at $\pm 128\gamma$ while the resolution changes from $1/16\gamma$ to $\pm 1/2\gamma$ in response to changes in the strength of the field.

The fact that the sample rate of the magnetometer will vary more than two orders of magnitude in the course of the mission from well above to well below the spin period of the magnetometer, required special attention in the data handling assembly. At sampling rates well above the spin frequency, the signals are filtered automatically to obey the Nyquist sampling criterion and sampled synchronously with the telemetry system. At low sampling rates the signals are sampled synchronously with the spin of the spacecraft and combined in such a way as to provide inertially referenced data before transmission to Earth.

20. Orbiter Plasma Analyzer (OPA)—J. Wolfe/ARC

The Orbiter Plasma Analyzer (OPA) is an electrostatic energy-per-unit-charge (E/q) spectrometer capable of measuring flux as a function of E/q and the incident direction of positive ions or electrons (McKibben *et al.*, 1976). The instrument is mounted on the Orbiter near the outer edge of the spacecraft equipment shelf so that it looks out in a direction parallel to a radial from the spacecraft spin axis. The view angle is 140° in a plane parallel to the spin axis and 15° in the plane normal to the spin axis.

The instrument's analyzer section consists of a nested pair of quadrispherical plates with a mean radius of 12 cm and a plate separation of 1.0 cm. Charged particles that pass through an entrance aperture, admitting them into the region between the quadrispherical plates, are deflected by an electrostatic field between the plates. Those particles whose E/q are within a range defined by the electrostatic field strength follow a curved path between the plates and exit from the region between the plates. They are then collected by an array of five current collectors located beyond the exit aperture. Each target is connected to an electrometer amplifier.

By varying the voltage difference between the plates, and hence the electrostatic field strength, a range of E/q values is covered for both positive ions and electrons. By covering a sufficiently large range of E/q values, the complete particle spectrum is then measured. The incident direction of the incoming particles is determined from the spacecraft azimuthal angle and the relative responses of the five targets. The range of E/q values for high energy positive ions is from 50 to 8000 V covered in 32 steps spaced logarithmically equal. For electrons and low energy positive ions the E/q range from 3 to 250 V is used, covered in 15 logarithmical steps plus a 'zero' step at 0.25 V. The 32 step range for ions is, for purposes of identification, labeled E_1. The 15 step range for electrons is called E_2 and the 15 step range for low energy ions is denoted as E_3.

The instrument has two commandable logic modes of operation, the scan mode, (M_1), and the step mode, (M_2). In the scan mode, (M_1), the instrument first

performs a maximum flux scan, (MFS), during which the value of the maximum flux, the collector number which observed the maximum flux, and the spacecraft azimuthal angle for the flux are determined for each E/q step of the selected energy range. Then a polar scan (PS) and an azimuthal scan (AS) are accomplished at the four consecutive E/q steps beginning with the step before the one in which the peak flux was measured in the MFS. A polar scan consists of the maximum flux and corresponding angular sector for all 5 collectors at a given E/q step. The azimuthal scan contains the flux measured in 12 azimuthal sectors centered on the peak flux direction for the collector which measured the peak flux in the polar scan (PS). The angular sectors are 1/512 of a spacecraft revolution in width. The angles of the sectors with respect to the maximum flux direction are 0°, $\pm 1\frac{13}{32}°$, $\pm 2\frac{13}{16}°$, $\pm 5\frac{5}{8}°$, $\pm 11\frac{1}{4}°$, $\pm 22\frac{1}{2}°$, and 180°. The polar scan and azimuthal scan are accomplished consecutively at each E/q step. In the step mode, (M_2) only the maximum flux scan (MFS) is done.

The instrument can be operated with any combination of mode (M_1 or M_2) and energy range (E_1, E_2 or E_3) by means of ground command.

21. Orbiter Electric Field Detector (OEFD) — F. Scarf/TRW

The electric field detector on the Pioneer Venus Orbiter will provide data to answer fundamental questions on the characteristics of the solar wind–Venus interaction at a level that is appropriate for a low-cost, Pioneer-type investigation of Venus. The instrument will give significant information on the mode of plasma interaction between the solar wind and the exospheric or ionospheric plasma (Cloutier *et al.*, 1969; Spreiter *et al.*, 1970), the variable locations of the Venus bow shock, ionopause and wake cavity boundary (Bridge *et al.*, 1967, 1974; Dolginov *et al.*, 1973; Gringauz *et al.*, 1973), the role of plasma instabilities in modifying the heat flux from the solar wind to the ionosphere (Scarf, 1970), the wave-particle interaction mechanisms that can cause 'pickup' or thermalization of upstream ions formed when atoms from the Venus exosphere are ionized in the streaming solar wind (Hartle *et al.*, 1973; Wallis, 1972), the extent of the upstream turbulence region, and the effects of wave-particle interactions within the Venus ionosphere. Secondary objectives involve a search for whistler mode electromagnetic noise bursts from the atmosphere and analysis of solar wind disturbances at the Venus orbit and in cruise.

A modified version of the VLF electric field detector now operating on Pioneer 8 (Scarf *et al.*, 1968), Pioneer 9 (Scarf *et al.*, 1971) will measure electric components of local plasma waves and radio emissions in the frequency region extending from about 50 Hz to 50 000 Hz. The OEFD includes a self-contained, balanced, Vee-type electric dipole antenna, a differential preamplifier, and four 30% bandwidth channels which are essentially the same as the bandpass channels from the Pioneer 8,9 instruments. The 66 cm long antenna elements are designed

to lean on the shroud and to deploy automatically in the spacecraft equatorial plane when the shroud is ejected.

The instrument will measure wave amplitudes in bandpass channels centered at 100 Hz, 730 Hz, 5.4 kHz, and 30 kHz. The significance (in terms of local characteristic plasma wave frequencies) of the individual bandpass channel measurements varies with position along the orbit. For instance in the bow shock, upstream solar wind and ionosheath regions, the mean plasma density should be between 5 and 50 cm^{-3}, and electron plasma oscillations will be detected in the 30 kHz channel, while ion acoustic waves and electron whistler mode waves will appear in the 100 Hz and 730 Hz channels; Figure 26 shows expected results from Venus, based on comparison with IMP-6 measurements at the Earth's bow shock (Rodriguez and Gurnett, 1975). Near periapsis the relations involving wave frequencies and local parameters are very different. For instance, when the density ranges between 2×10^4 and 4×10^4 cm^{-3}, ion acoustic waves associated with CO_2^+ ions in the ionosphere will be detected at 5.4 kHz (see Figure 27). At all orbital locations it is expected that electron whistler mode signals from the atmosphere can be detected in the 100 Hz channel.

22. Orbiter Cloud Photopolarimeter (OCPP) — J. Hansen / GISS

The OCPP employs a 3.7 cm diameter telescope for spin-scan mapping of the planet in different spectral bands. Observations will be made at fixed look angles, using spacecraft rotation to generate scans across the planet and using motion in

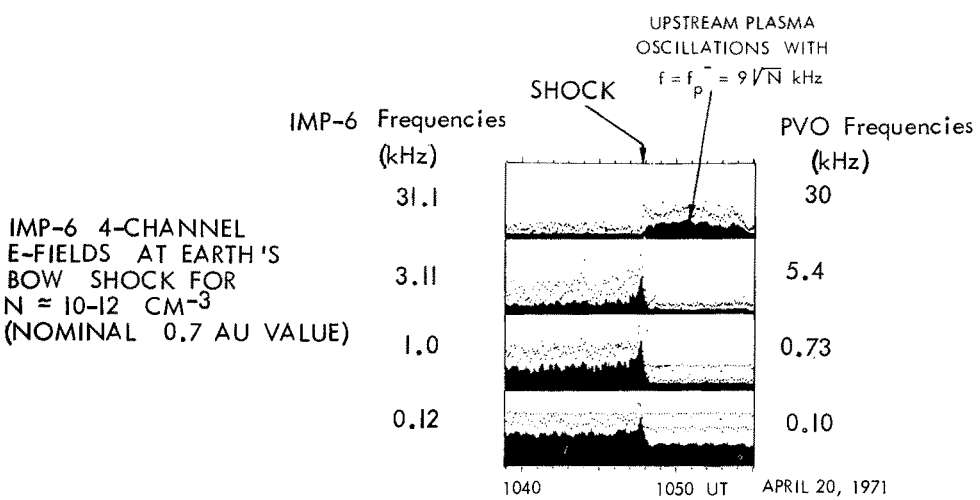

Fig. 26. (OEFD). IMP-6 measurements of plasma waves at the Earth's bow shock in four frequency channels selected to show how the Pioneer Venus instrument should respond when the Venus bow shock is laminar, with upstream disturbances generated only by electrons. Whenever exospheric atoms or backstreaming protons lead to suprathermal ions upstream from Venus, then a very thick type of interface region should develop.

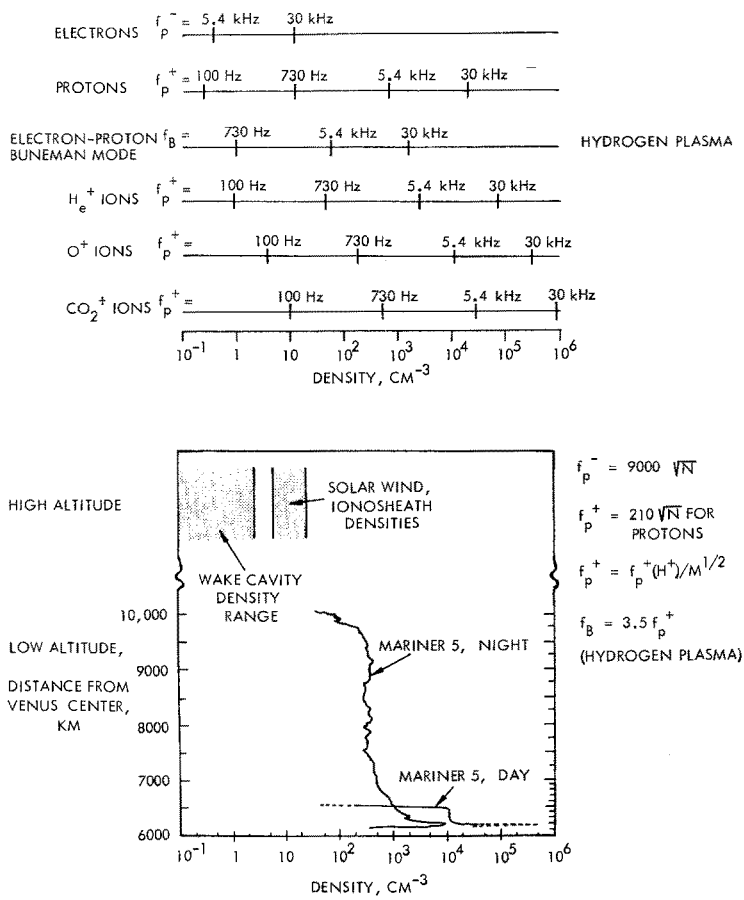

Fig. 27. (OEFD). Characteristic frequencies for density-dependent plasma wave modes ($f_p^{\pm}$, f_B), with markings designating the frequency locations of the four OEFD bandpass channels.

orbit for cross-scan coverage. The look angle of the telescope can be varied to allow observations of the planet from any point in the orbit.

The optical elements of the OCPP are shown in pictorial fashion in Figure 28. The optical components of the telescope include a filter-retarder wheel with 16 active positions, a Wollaston prism and 4 photodiode detectors. Table IX gives the OCPP instrument parameter summary.

In the imaging mode of operation the field-of-view is about $\frac{1}{2}$ mrad, corresponding to a typical resolution of about 30 km at the subsatellite point. Only the intensity (radiance) is measured in this mode. Approximately $3\frac{1}{2}$ hr are required to complete one image of the full planetary disk; thus five full images can be obtained in the 18 hr of the orbit centered on apoapsis. A higher frequency of observation for a given region on the planet will be obtained by restricting the

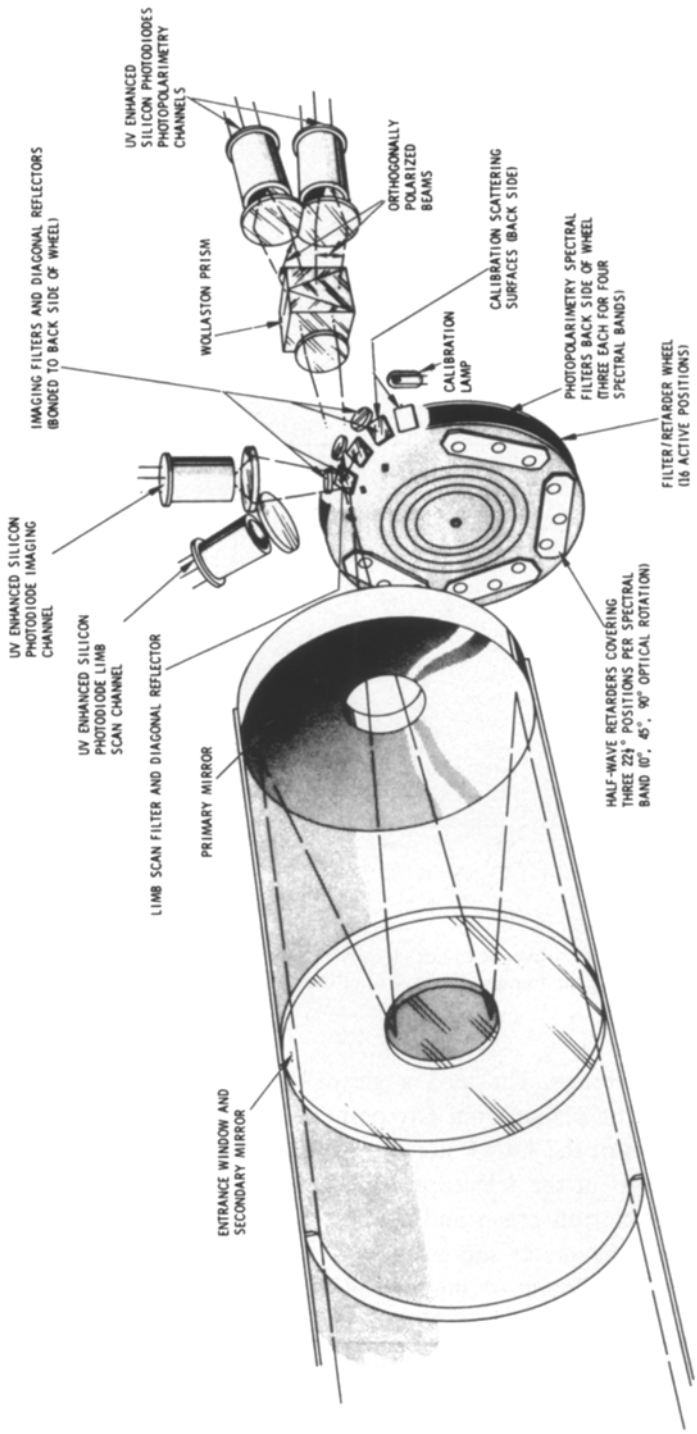

Fig. 28. (OCPP). Pictorial view of the optical system of the OCPP.

observations to a correspondingly smaller fraction of the planetary disk. Throughout the mission, but particularly during the period from 30 to 130 days after orbit insertion, there will be several periods of concentrated imaging to record atmospheric changes for the range of available time scales.

In the photopolarimetry mode the field-of-view is about one-half degree, corresponding to a typical resolution of about 500 km at the subsatellite point. Four passbands centered at 265, 365, 550 and 925 nm are used in this mode; the intensity, degree of polarization and direction of vibration are determined for each of these. Cloud and haze particle size, shape and refractive index for local areas on the planet will be extracted from the photopolarimetry measurements as a function of scattering angle and wavelength. The vertical distribution of cloud and haze particles as a function of atmospheric pressure will be extracted down to a cloud optical depth of about unity from the photopolarimetry measurements as a function of zenith angle. The required ranges of scattering angle and zenith angle will be obtained by means of observations of local areas from several different points in a given orbit.

In the limb-scan mode the field-of-view is about $\frac{1}{4}$ mrad. These high resolution limb-scanning observations will be made in the periapsis portion of the orbit with a typical resolution of $\frac{1}{2}$ to 1 km. The observations will be used to obtain information on the vertical distribution of high haze layers down to the level at which the vertical optical depth is about 0.1.

23. Orbiter Infrared Radiometer (OIR)—F. Taylor/JPL

The Orbiter Infrared Radiometer (OIR), is an eight-channel radiometer for vertical temperature sounding of the stratosphere and mesosphere of Venus. Five channels in the ν_2 band of carbon dioxide near 15 μm wavelength are used for temperature sounding. One of these is adjustable on command from Earth to be sensitive to radiation originating from three different levels in the mesosphere, allowing temperature measurements to be made in a total of seven independent atmospheric layers. The range of altitude and pressure covered by the vertical soundings is from about 60 km and 250 mb at the top of the dense clouds, out to approximately 150 km and 10^{-6} mb. This range encompasses the four-day circulation regime, the regions of maximum cooling to space and maximum deposition of solar energy, and most of the ionosphere. Two of the eight channels are used for investigations of the cloud morphology and measurement of the Bond albedo. The eighth channel is used to detect and map the distribution of water vapor in the Venusian atmosphere. Further discussion of the principles of remote sounding of the atmosphere of Venus, and methods for the retrieval of the parameters of interest from radiometric measurements, may be found in the paper by Houghton and Taylor (1974).

Figure 29 illustrates the selection of spectral bands for the radiometer. The wide range spanned by these (from the ultraviolet to the far infrared) calls for

TABLE IX
Cloud photopolarimeter (OCPP) instrument parameter summary

Parameter	Characteristic		
Telescope	Dall-Kirkham, 3.7 cm aperture, 15.7 cm focal length		
Look angle selection	Telescope slews to one of 64 commandable look angles for data taking		
Starting roll position	Selectable to be any one of the 256 spokes into which roll is divided		
Memory storage	First in/first out 8192 bit memory (3072 bit section used in photopolarimetry mode)		
Commands	Power on/off; photopolarimetry mode; imaging mode; limb scan mode; one quantitative command for gain, roll position, look angle position, low sample rate, alternate roll readout, DC-restore position, redundant imaging, and low step rate.		
Interface signals (to OCPP)	Four commands plus power on/off; roll reference pulse; sector pulses (1024/roll); clock (32.8 kHz); read clock; read envelope; digital signal return; 28 V power and return		
Interface signals (from OCPP)	Digital science data, digital sub-com data, digital signal return		
Viewing and pointing requirements	Unobscured view within 10° of OCPP telescope optical axis at all look angles between 35° and 155°		
Temperature limits	−7° to +40°C (operating): −18° to +50°C (nonoperating)		
Size	22×28×46 cm		
Modes of operation	Photopolarimetry	Imaging	Limb scan
Spectral bands	265 nm (250–280): 365 nm (350–380): 550 nm (545–555): 925 nm (920–930)	Detects wavelengths less than 390 nm	Within 500–800 nm spectral interval

Instantaneous field of view	6.5×8 mrad (rectangular)	0.4×0.5 mrad (rectangular)	0.2×0.25 mrad (rectangular)
Detectors	Two UV-enhanced silicon photodiodes operated in photovoltaic (unbiased) mode	One UV-enhanced silicon photodiode operated in photovoltaic (unbiased) mode	One UV-enhanced silicon photodiode operated in photovoltaic (unbiased) mode
Polarization analyzer and calibrator	Symmetrical Wollaston prism analyzer and four half-wave retardation plates	Not applicable	Not applicable
Radiometric calibration	Solar diffuser; inflight reference calibrator	Solar diffuser	Solar diffuser
Analog/digital conversion	11 bit a/d conversion of the two analog signal channels	8 bit a/d conversion of analog signal channel	8 bit a/d conversion of analog signal channel
Sampling rate	Two signal samples sampled simultaneously every 9.52 ms (28.6 ms with low sample rate)	Signal channel sampled every 0.488 ms (0.610 ms with low sample rate)	Signal channel sampled every 0.310 ms (0.397 ms with low sample rate)
Data format	56 bits status followed by 3016 bits data	56 bits status followed by 8136 bits data	56 bits status followed by 8136 bits data
Angular swath sampled	39.2 at 5 RPM (memory fill; 6.5×8 mrad aperture); 117.5 with low sample rate	14.9 at 5 RPM (memory fill); 18.1 with low sample rate	9.3 at 5 RPM (memory fill); 12.1 with low sample rate
Measurement accuracy	Polarimetric: ±0.2% (±0.3% for 270 nm) absolute radiometric: ±5% (precision better than 1%)	Absolute radiometric: ±5%	Absolute radiometric: ±5%

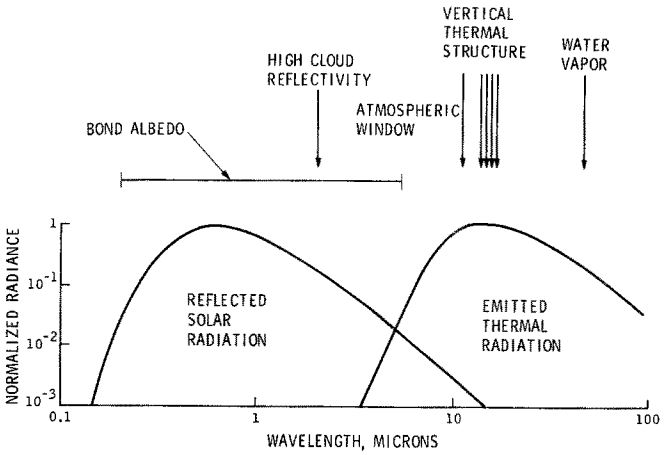

Fig. 29. (OIR). Infrared Radiometer spectral band selection.

several different measurement techniques to be integrated into a single instrument. Channel 1 uses the pressure–modulation technique (Taylor *et al.*, 1972) which was developed for the PMR experiment on the meteorological satellite Nimbus 6. In this, a cell containing CO_2 gas itself is used as the spectrally selective element. In addition to modulation of the CO_2 pressure at approximately 40 Hz by means of a resonant piston, slow changes in the mean cell pressure may be produced by heating or cooling a molecular sieve attached to the cell. The latter provides for commandable changes in the height at which the channel 1 weighting function peaks in the atmosphere. In this way, channel 1 can be used to measure temperatures anywhere from the temperature minimum near pressures of 10^{-2} mb up to the beginning of the exosphere, where dissociation of CO_2 by solar extreme ultraviolet radiation becomes important and non-LTE radiation processes dominate. The pressure modulation unit and molecular sieve, which make up channel 1 of the radiometer, are visible in the foreground of Figure 30, which is an isometric drawing of the instrument. These devices have been developed and fabricated by Oxford University in England, for integration into the rest of the radiometer at the Jet Propulsion Laboratory.

Figure 30 also shows the fixed grating monochromator which is used to select the remaining 15 μm band channels, numbers 2 through 5. Channel 6 uses a narrow band interference filter centered on the 2.0 μm CO_2 bands in the near infrared; differentiation between clouds at different levels in the atmosphere is by measurement of the opacity of the intervening CO_2. Channel 7 is the wide-band albedo channel (0.20 to 4.5 μm) which measures the spatial and angular variation in total reflected solar intensity. Channel 7 uses absorption filters to determine a flat optical band and residual reflections for attenuation. Channel 8 is centered on the strongest part of the pure rotational band of water vapor (40 to 50 μm) and is

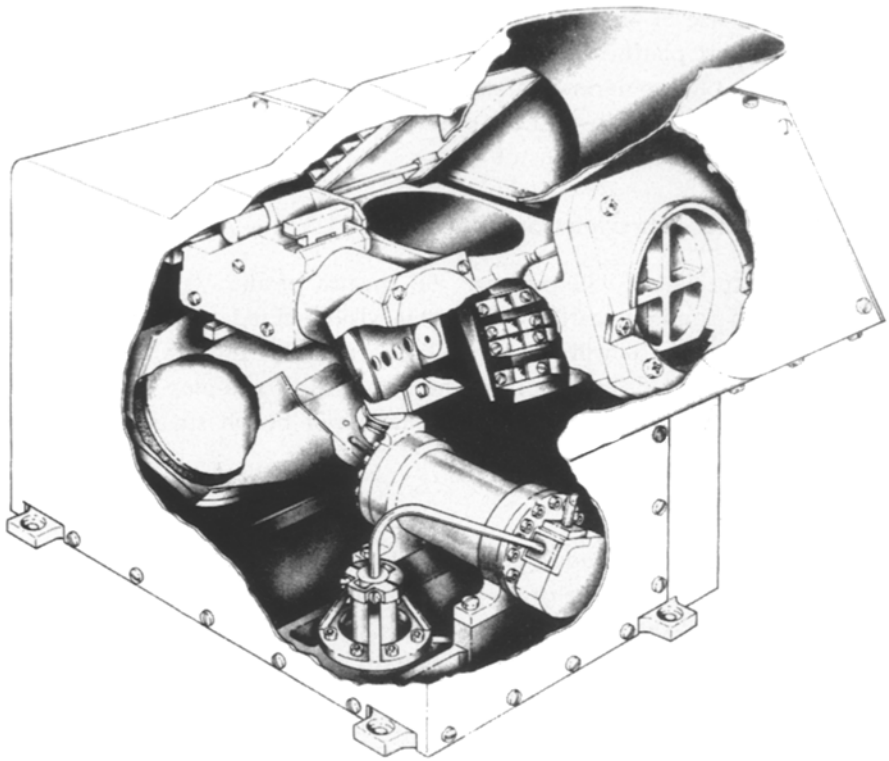

Fig. 30. (OIR). Venus Orbiter radiometric temperature sounder.

defined by three reststrahlung reflections from barium fluoride and the transmission of a silicon lens.

All of the channels are fed by a 48 mm aperture off-axis parabolic telescope mirror and observe Venus with a 1.25° field of view (5° for channel 1). This narrow field of view, combined with the close approach of the spacecraft to the planet, results in a spatial resolution which is a few km near periapsis. The sample time (nominally 30 ms) is kept small in order to avoid smearing of the field of view by the spinning motion of the spacecraft, but large enough to obtain signal to noise ratios of at least 100 in all channels. This corresponds to a temperature sensitivity of better than 0.5 K at 240 K.

Specially designed logic circuits incorporated into the instrument sense the crossing of the limb of the planet and reduce the dwell time to 12 ms for a period of about 150 ms during the time that the radiometer is viewing the atmosphere tangentially at the limb. This technique, similar to that applied by the LRIR experiment on Nimbus 6 to the Earth's stratosphere and mesosphere, is useful for obtaining additional vertical resolution over a limited altitude range. Here the goal is to obtain additional information on cloud stratification and the vertical distribution of water vapor.

The physical size of the OIR instrument is $24.8 \times 17.5 \times 25.1$ cm. It is mounted on the instrument platform to view at a fixed angle of 45°, boresighted in one plane with the photopolarimeter and the ultraviolet spectrometer instruments. Mounted in this way the instrument obtains the most equitable coverage of both the polar and equatorial regions of Venus.

24. Orbiter Ultraviolet Spectrometer (OUVS) — A. Stewart/Colo.

The OUVS experiment will measure the spectra of the Venus day and night airglow, and of sunlight scattered from the visible cloud tops, haze layers, and nearby atmosphere. It will measure limb intensity profiles and disk trace brightnesses of selected features from these spectra. It will map Venus' hydrogen corona out to 11 R_{φ}. In all studies emphasis will be on spatial and temporal variations.

24.1. Instrument

The OUVS instrument includes: a light shade, a telescope, and a monochromator with a programmable grating drive and two exit slits; two photomultipliers with pulse amplifiers and shapers; data pulse counters, word compressors, and a buffer; and a control subsystem that allows instrument mode and parameters changes by ground command (Figure 31).

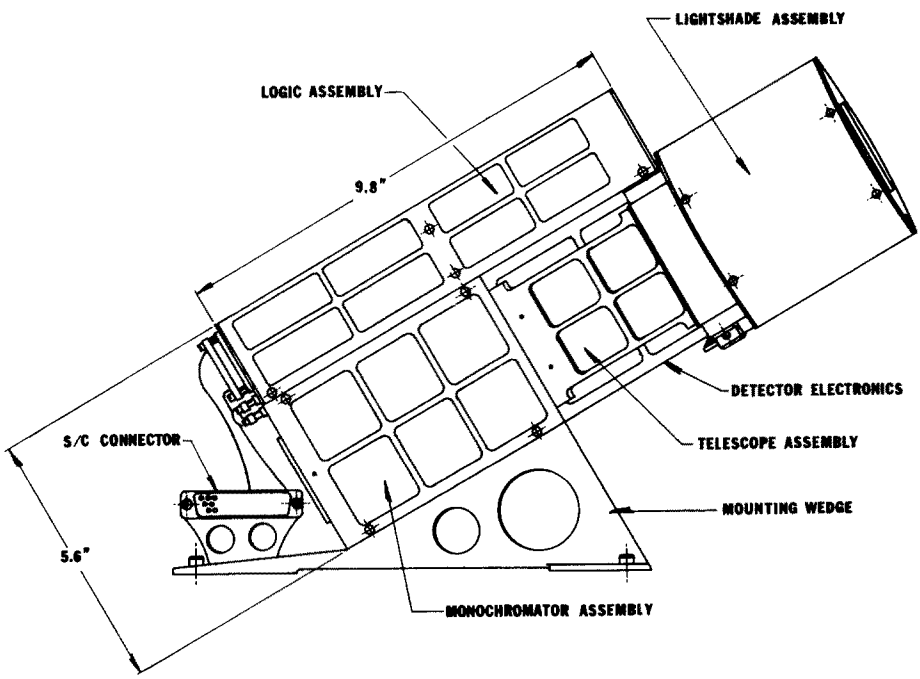

Fig. 31. (OUVS). Orbiter Ultraviolet Spectrometer.

24.2. Descriptive summary

Telescope: 250 mm f/5 Cassegrain 1.83°×0.16° field of view.
Monochromator: 125 mm f/5 Ebert-Fastie; 3600 line mm^{-1} diffraction grating; 15 A spectral resolution; 4.4 A grating steps.
Detectors: Channel 1: CsI cathode, LiF window, 1100–1900 A; Channel 2: CsTe cathode, SiO_2 window, 1900–3600 A; Counting capacity: up to 2 MHz.
Data Store: 256 words
Viewing: 60° from spin axis

24.3. Commandable functions and parameters

Grating drive: scan, or fixed at any one of 512 positions.
Data channel: select Channel 1 or Channel 2.
Integration period: select 4, 8, 16 or 32 ms.
Spatial reference pulse: select Ram, Nadir, or Inertial pulse from S/C, or Rising or Falling Limb from internal limb sensor
Data delay: select 0–360° delay between receipt of spatial reference pulse and start of data-taking.

24.4. Sensitivity and dynamic range

Thresholds are determined by the dark current, and upper limits by counter capacities. The long wavelength upper limits for continuum brightness reflect an automatic ×20 gain reduction.

Wavelength, Å	*Line Emission*	*Continuum*
1216	4R–1.5MR	—
1304	3R–1.0MR	—
1657	13R–4.5MR	—
2160	7R–1.8MR	0.5R–2.5MR $Å^{-1}$
2890	20R–5MR	1.3R–7MR $Å^{-1}$
3400	—	10R–50MR $Å^{-1}$

24.5. Operational modes

Spectral Mode: the complete spectrum is scanned in four 256 word sections. Each section takes one S/C spin to collect, store, and read out into the telemetry stream.
Wavelength Mode: the grating position, data channel, spatial reference pulse, and data delay are selected by ground command. Normally a 30° arc of data is collected, stored, and read out during each S/C spin.
Lyman-alpha Mode: individual measurements at a fixed wavelength are made and delivered to the telemetry system upon demand.

Back-up Modes: two additional modes are available in which the instrument functions without using its command capability or its data buffer.

24.6. Nominal orbital operations

The planet is in view starting about two hours before periapsis and ending a few minutes after periapsis. The approach phase will be used for airglow and cloud disc traces. Near periapsis, the long axis of the field of view is approximately parallel to the planet's limb, and airglow limb intensity profiles and limb haze scattering profiles will be measured. Spectra will also be recorded near periapsis.

While the planet is out of view, the Lyman–alpha mode will be used to map the hydrogen corona at a low rate ($\sim$2 measurements min^{-1}).

25. Orbiter Radar Mapper Instrument (ORAD)—G. Pettengill/MIT

The prime objective of ORAD is to obtain a large number of altimetry measurements along the suborbital track to the highest feasible spacecraft altitude. Primary power available to ORAD is 30 W and the maximum antenna diameter that can be accomodated is 38 cm. An S-Band system (1.757 GHz) with a peak pulse power of 20 W and 14 dB antenna gain (30° beamwidth) will provide usable signal returns to about 3000 km altitude, for a surface specular reflection coefficient of 10 dB.

The antenna must be moved in a plane containing the spin axis to view the subsatellite point on the planet surface once during each spacecraft roll. This angle will vary from 15° to about 140° during a given radar pass. This led to the choice of a mechanically pointed antenna mechanism and the need to mount the antenna on the periphery of the spacecraft equipment shelf. For a spacecraft spin rate between 4.9 and 5.1 RPM, the radar observation interval will last only about one second out of the spacecraft roll period of 12 s.

ORAD compensates, on the basis of telemetered ephemeris information, for Doppler shift associated with its vertical (i.e., radial) motion. In addition, below 700 km, the received frequency is sequentially tuned to several values slightly above and below the nadir value of Doppler shift to allow range measurements of areas lying just ahead and behind the nadir location during a single roll.

Relatively long-duration pulses are used to obtain a satisfactory single pulse signal-to-noise ratio; these pulses must be modulated (coded) to provide reasonable values of range and surface resolution. Adequate signal levels are provided by a 55 baud (sub-pulse) code with a baud duration of 4 μs for the altitude range from periapsis to 1500 km; above 1500 km the baud duration is increased to 6 μs. Four values of pulse repetition frequency (PRF) will be programmed as a function of altitude as shown in Table X. These PRF's produce a four-fold range ambiguity between 3000 and 2575 km altitude, and two-fold ambiguity between 2575 and 1515 km, becoming unambiguous below 1515 km. Blind ranges are averted by changing PRF's at appropriate altitudes.

TABLE X
PRF schedule and baud duration *vs.* altitude

Altitude (km)	PRF (Hz)	Baud (μs)
3000 to 2575	189.4	6
2575 to 1515	108.2	6
1515 to 700	92.8	4
Below 700	189.4	4

Four Doppler filters will be implemented for spacecraft heights below 700 km to provide the multiple along-track altimetry measurements. Above 700 km, operation will be restricted to one nadir measurement per roll. The choice of instrument parameters and spacecraft velocity produces the resolution cell pattern shown in Figure 32, for which a spherical planet surface is assumed. The four Doppler bands will be offset as shown by shifting the transmitter frequency during the one-second view period. Table XI indicates the variation in resolution cell dimensions with altitude. The cell radius refers to the cross-track dimension (circles in Figure 32) and the filter widths correspond to the strips marked F. At

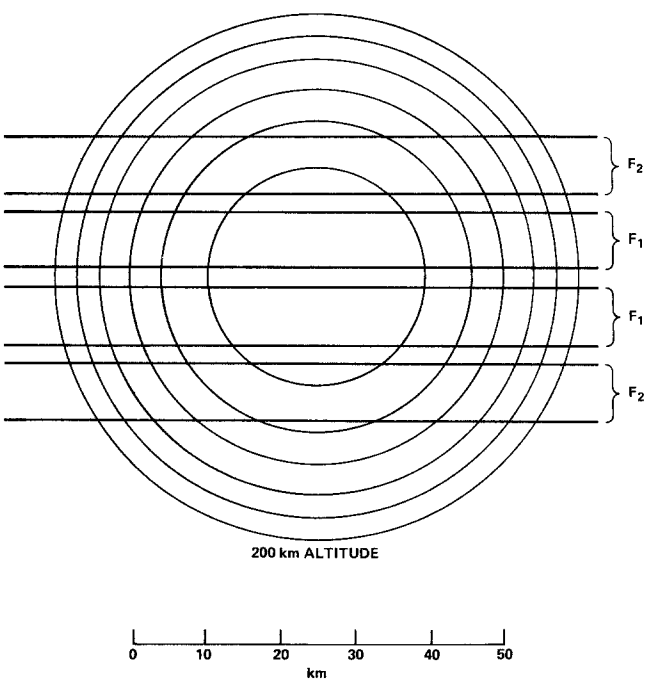

Fig. 32. (ORAD). Range and Doppler resolution cells for altimetry.

TABLE XI
Resolution cell dimensions *vs.* altitude for altimetry

Altitude (km)	Cell radius (km)	Filter width (km)	Filter center offsets from nadir (km)	
			Inner	Outer
200	15.2	7.9	5.2	15.8
300	18.5	12.1	8.1	24.2
400	21.2	16.4	10.9	32.8
500	23.5	20.8	13.8	41.6
600	25.6	25.4	16.8	50.8
800	29.1	34.8	—	—
1000	32.1	44.8	—	—
1500	46.5	48.0	—	—
2000	52.0	68.2	—	—
2500	56.4	90.7	—	—
3000	60.0	115.2	—	—

the higher altitudes the signal return area will be determined almost entirely by the range dimension.

The functional parameters for altimetry measurements are altered for the imaging operational mode for altitudes below 500 km altitude. The imaging mode uses uncoded pulses at a 250 Hz PRF to provide a 500 km unambiguous range and commands the measurements prior to antenna passage through nadir to prevent surface mapping ambiguity. Thus, a sequence of surface images overlapping roll-to-roll parallel to the ground track are built up. The imaging can be performed on one or both sides of the ground track, as selected by ground command. A pulse duration of 120 μs was chosen so that the image resolution cell dimensions in Doppler and range are approximately equal at 500 km. Equality of these dimensions is maintained for lower altitudes by starting the imaging process at larger roll-angle offsets from nadir (the offset is about 19° at 500 km altitude, increasing to about 38° at periapsis). The received signal is subdivided into eight intervals to provide eight cross-track range circles. Each subinterval sample is processed in an eight-point Fast Fourier Transform circuit to yield filtering with about 8 kHz spacing. Thus, the surface area illuminated is in effect subdivided into 64 resolution cells or pixels as represented in Figure 33. Incoherent integration of 125 returns is planned to insure an adequate signal-to-noise ratio. Typical center-scene resolution-cell dimensions, and their variation with altitude are shown in Table XII. On-board processing of the imaging data reduces the telemetry requirements to a level consistent with the spacecraft capability and requirements of the other Orbiter experiments. With 10 bit quantization, only 640 bits are acquired each roll.

The ORAD altimeter design is an 'open-loop' operation, compared to the more conventional approach using range tracking of the target. Ground tracking will

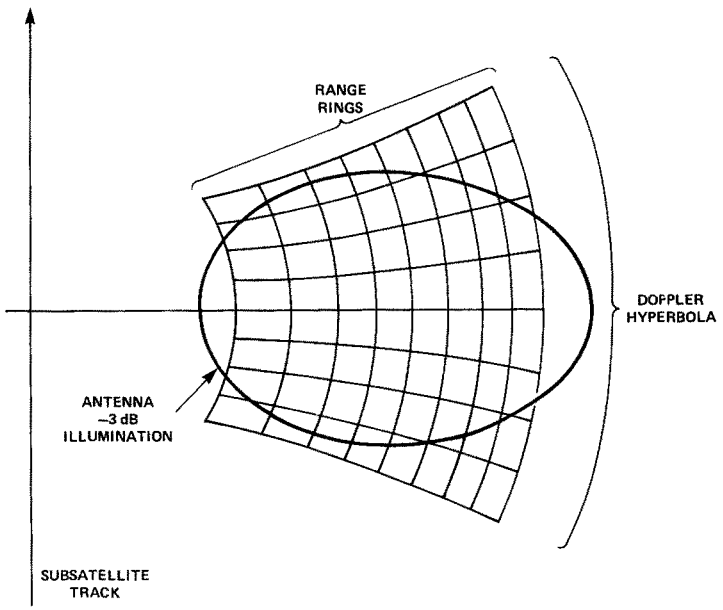

Fig. 33. (ORAD). Representative scene mapped in imaging mode.

establish the spacecraft ephemeris from which *a priori* estimates of the range to the planet surface can be obtained. Hence, it is sufficient to send by uplink telemetry, a range 'window', programmed in time, sufficiently large to encompass worst-case variations in surface heights. The ORAD 'window' has been selected to be 64 one-baud range cells, providing a range depth of nearly 40 km for the 4 μs baud and about 60 km for the 6 μs baud. For altitudes less than 700 km, the time to peak signal return with respect to the start of the window will be telemetered for each of the four Doppler bands. At higher altitudes only the nadir Doppler band is observed. The signal amplitudes will be telemetered using ten-bit quantization in each of 17 range bins, starting at six bins prior to the one containing the signal peak. Also, by ground command, the low altitude Doppler filtering can be disabled, thereby providing, in effect, four successive nadir measurements displaced only by the spacecraft motion. This should be useful in the event particularly anomalous surface characteristics are encountered.

26. Orbiter Gamma-Ray Burst Detector (OGBD)—W. Evans/LASL

26.1. Objectives

The purpose of the gamma-ray burst experiment is to provide observations of intense, short duration emissions of high energy photons from astronomical sources. The discovery of this phenomenon is very recent (1973) and the nature and location of the sources are still unknown. By correlating the time of arrival of the gamma bursts at widely separated detectors it is possible to derive precise information on source direction. The Venus Orbiter spacecraft provides an

TABLE XII
Center scene resolution cell dimensions for imaging

Altitude (km)	Resolution range	Cell dimensions (km) azimuth
500 (Approaching periapsis)	35.5	43.3
400	31.1	37.9
300	27.0	22.7
200	23.0	26.0
300 (Leaving periapsis)	27.0	28.1
400	31.1	33.5
500	35.5	39.0

experiment platform separated from the Earth by ~1 AU. Correlations with near-Earth observations can provide directional determinations with accuracies less than one arc minute – sufficient for a meaningful attempt at optical identification of the sources.

26.2. Concept and approach

The gamma bursts occur randomly in time (~10 per year above the detection threshold of existing spacecraft instruments) and, from the limited direction information presently available, the sources are random in direction. No firm evidence now exists for repeated bursts from the same source. These conditions dictate a detector system with a maximum field of view that provides continuous (in time) observations. The OGBD experiment consists of two NaI photomultiplier detector units mounted to provide nearly uniform sensitivity over a 4π steradian field of view. The detectors are sensitive to photons in the 0.2 to 2.0 MeV energy range and provide coarse spectral information with a four-channel pulse height analysis. The gamma bursts are very intense and last for only a short time (one-tenth second to a few tens of seconds). To accomodate the very high data rates that occur during an event, the experiment includes a buffer memory of 20 k bits for storing the event data for later read out. Internal logic continuously monitors the count rate and detects the rapid increase in count rate that signals the beginning of a gamma burst.

26.3. Measured parameters

The detector will provide a continuous time history of the gamma-ray flux for those events intense enough to be detected. A four-channel pulse height spectrum will also be obtained during an event. Continuous measurements of the observed counting rate (with much lower time resolution) will provide a data base for searching for 'slower' transient events, whose rise times are not sufficiently fast to trigger the detection logics.

26.4. Accuracies and Limitations

The uncertainty in directional determinations derived from long baseline 'triangulation' is given by

$$\Delta\theta = \frac{c}{s \sin\theta}\Delta\tau$$

where c = speed of light, s = spatial separation between two detectors, θ = angle between the line joining the detectors and the source direction, τ = difference in the arrival time of the signal at the two detectors. The time difference τ is determined by maximizing the function

$$f(\tau) = \int_0^\infty f_1(t) f_2(t+\tau)\,\mathrm{d}t$$

where f_1 and f_2 are the observed fluxes at the two detectors. The uncertainty in τ depends on (1) the accuracy with which an absolute time base can be associated with the two functions f_1 and f_2, (2) the statistical precision of the two functions f_1 and f_2 and (3) the 'shape' of the two functions (i.e. the more 'spiky' the functions, the more pronounced is the maximum in $f(\tau)$). For correlations of the OGBD experiment at 1 AU with a near-Earth experiment the angular uncertainty $\Delta\theta$ is expected to be less than one arc minute under worst conditions and of the order of 10 arc seconds for events of 'average' intensity.

27. S and X-Band Radio Occultation Studies of the Atmosphere and Ionosphere of Venus (ORO)—A. Kliore/JPL

The radio occultation method for studying planetary atmosphere is well known and has been applied to measure the atmospheres of Mars, Venus and Jupiter. Sometimes the method is called radio-transillumination or radio-eclipse. It consists of observing signals from the spacecraft as they penetrate an atmosphere and ionosphere of a planet. The refractive index profile and absorptivity of the planetary atmosphere determine the phase and amplitude changes that are observed in a signal that reaches the Earth. The application of integral inversion procedures provides a profile of the index of refraction in the atmosphere and of the electron density in the ionosphere, as well as the absorptivity. The absorptivity measured at the two frequencies allows one to determine the existence of absorbing and scattering layers associated with clouds in the atmosphere.

The approximately 80 occultations which the Pioneer Venus Orbiter will provide will produce about 160 refractivity profiles in the lower atmosphere of Venus down to the level of critical refraction, from which pressures, temperatures and densities will be computed. The accuracy of the measurements taken during exits from occultation will depend on the stability of the spacecraft oscillator.

Simultaneously, the electron density distribution will also be measured above these 180 locations in the atmosphere of Venus from the dispersive differential

Doppler effect observed at the two frequencies. This will yield information on the changes in electron density profiles with latitude, longitude and solar illumination angle. Since most of these measurements will be made on the night side of Venus, it will produce data on the reportedly variable Venus night time ionosphere.

Measurements of the amplitude fluctuation of the S and X-band signals will be used to study the radio absorbtion structure of clouds and their variabilities with latitude.

Horizontal pressure and temperature gradients and pressure and density oscillations produced from the occultation profiles will also be used to study the dynamics of the lower atmosphere of Venus with respect to the 24 hr sampling time of the orbit.

The experiment will be conducted by using the spacecraft transponder equipped with a coherent X-band transmitter and a despun orientable high-gain antenna which will be able to follow the refracted position of the radio ray during occultation. In addition, the Deep Space Net stations on the Earth will be equipped with special receivers with the capability of varying their reference frequency by means of digitally controlled programmable oscillators.

28. Orbiter Dual-Frequency Experiments (OGPE)—T. Croft/SRI

28.1. Radio occultations

The amount of information returned from Orbiter occultations is much greater than that which can be derived from a single spacecraft passage behind a planet. Each occultation provides a record of signal Doppler shift and strength versus time; the interpretation of one such record hinges upon the assumptions which the investigator chooses to make concerning the character of refractive index variations with respect to directions other than the local vertical. Typically, these variations are assumed to be non-existent, allowing the use of spherical symmetry which greatly simplifies the mathematics and permits the ray propagation equations to be inverted. (That is to say, it then becomes possible to calculate refractive index versus height by direct manipulation of the Doppler shift–time relationship.)

The path repetitively followed by the Venus Orbiter is comparatively unchanging with respect to a non-rotating frame of reference which travels with the center of the planet. However, the motion of Venus and Earth in their orbits around the Sun leads to a daily progression of the occultation points around the limb of Venus. It follows that the expected 160 occultations (a daily entry and exit for 80 days) will occur at points which are separated from one another by distances on the order of 100 km. The separations are smaller at the beginning of the mission and they gradually increase. All latitudes are sampled from the North Pole to approximately 60° south. The major limitation of the orbits lies is the absence of daytime occultations, with the exception of a few which are at polar latitudes.

The multiplicity of occultations at Venus should permit detection of horizontal structure in the ionosphere (expected to be large) and in the atmosphere (expected to be small). Plans for interpretation rely in part on the use of computer simulation methods which take into account the three-dimensional gradient of refractive index; variations from symmetry will be tested using raytracing based on Hamilton's equations applied to a three-dimensional model. When horizontal gradients are thus allowed in the calculation, a unique solution cannot be found from a single occultation. An attempt will be made to construct self-consistent Doppler profiles from rays calculated in an asymmetric model, fitting them to a family of neighboring occultations.

28.2. Scintillation

Just as the Earth's atmosphere causes stars to twinkle, so does turbulence in the solar wind cause radio tracking signals to scintillate. The observation and analysis of radio signal strength and phase variations can shed light on the nature of the turbulence and, for this purpose, the S- and X-bank signals from the orbiter will be observed late in the mission when Venus approaches superior conjunction. At that time, the signal from the orbiter to Earth will pass through the corona/solar wind near the Sun where the plasma is dense enough to be effective.

The scintillation is caused by spatial inhomogeneity in the refractive index which depends in part upon the distribution of free electrons and in part upon the signal frequency. Turbulence in more tenuous plasmas can be detected with radio signals at lower frequencies, such as the 50 and 423 MHz system which was used for this purpose by Pioneer 9 out to 1 AU. The Soviets have made such observations using their tracking frequency near 940 MHz. American interplanetary spacecraft have made many such observations at S-band. Dual-frequency S–X observations (2300–8400 MHz) were initiated by Mariner 10 and continued by Viking. New observations by Pioneer Venus are desirable for two reasons: first, the corona is so changeable that a single series of observations by one spacecraft does not reveal how turbulence varies with respect to heliocentric distance. To learn such spatial relations, one needs several measurements in order that the spatial and temporal variabilities can be separated. Second, the evolution of interplanetary exploration by many nations has led to an ever-changing population of solar observing instruments on Earth and in space. At any given time, a new body of data offers new prospects for correlative studies of solar outbursts that happen to occur. The observation of an exceptional event by many different instruments increases our understanding of the character and propagation of the solar wind and, thus, our understanding of the Sun, other stars and of the action of the Sun upon the Earth and Venus.

As discussed in Section 14, (MPRO), the scintillation during occultations is expected to be evident and will be analyzed to determine the character of ionospheric and atmospheric turbulence. The study by this means is limited to altitudes above the critical level which is some 34 km from the surface. (Any radio

ray which penetrates this level can reach Earth only by means of reflection off the surface of Venus.) One of the most difficult aspects of the analysis of this form of scintillation is the separation of those signal variations which are due to atmospheric layering from those due to turbulence or other inhomogeneity of a comparable scale.

29. Atmospheric and Solar Wind Turbulence Experiment (OTUR)—R. Woo/JPL

Turbulence and ionospheric irregularities in the Venus atmosphere will be studied by analyzing the S- and X-band radio scintillations observed during radio occultation.Using recently demonstrated techniques we will measure the variation of the intensity of turbulence with altitude at different latitudes and longitudes as well as the distribution of scale sizes of turbulence (Woo *et al.*, 1974; Woo, 1975a). Measurements of electron density irregularities in the Venusian ionosphere will also be made (Woo and Yang, 1976).

Significant advances have been made in recent years in the use of phase scintillations (Woo, 1975b; Woo *et al.*, 1976a) and spectral broadening measurements (Woo *et al.*, 1976b) to study the solar wind. These techniques along with multiple receiving station observations will yield measurements of solar wind velocity, density fluctuations and structure in the solar wind over heliocentric distances ranging from a few solar radii to more than 1 AU.

30. Orbiter Atmospheric Drag Experiment (OAD)—G. Keating/LRC

The low periapsis of the Orbiter provides an opportunity to obtain the first spacecraft drag measurements of the atmosphere of another planet. The entire spacecraft, which is essentially in the shape of a cylinder, acts as the instrument. The effects of drag are obtained from Doppler measurements of the X and S band data being transmitted from the satellite. Atmospheric density is determined in the vicinity of periapsis, where the drag effect is much greater than elsewhere along the orbit, by correcting predicted changes to match observed changes of the orbit due to drag. The method by which this is accomplished is shown in Figure 34. The basic input are Deep Space Network (DSN) Doppler Measurements, spacecraft mass, spacecraft orientation, and an atmospheric model based on feedback from the drag experiment and other information on the atmosphere. From the spacecraft orientation, the cross-section presented in the direction of motion is determined. The drag coefficient in free molecular flow is determined from knowledge of the spacecraft orientation relative to the velocity vector and knowledge of relative composition based on the atmospheric model. The drag coefficient determination will be refined by experiments with molecular beams of carbon dioxide.

Two methods are envisioned for obtaining drag effects from the Doppler measurements. The primary method is to measure the orbital decay due to drag effects. This involves first obtaining orbital elements from the Doppler measure-

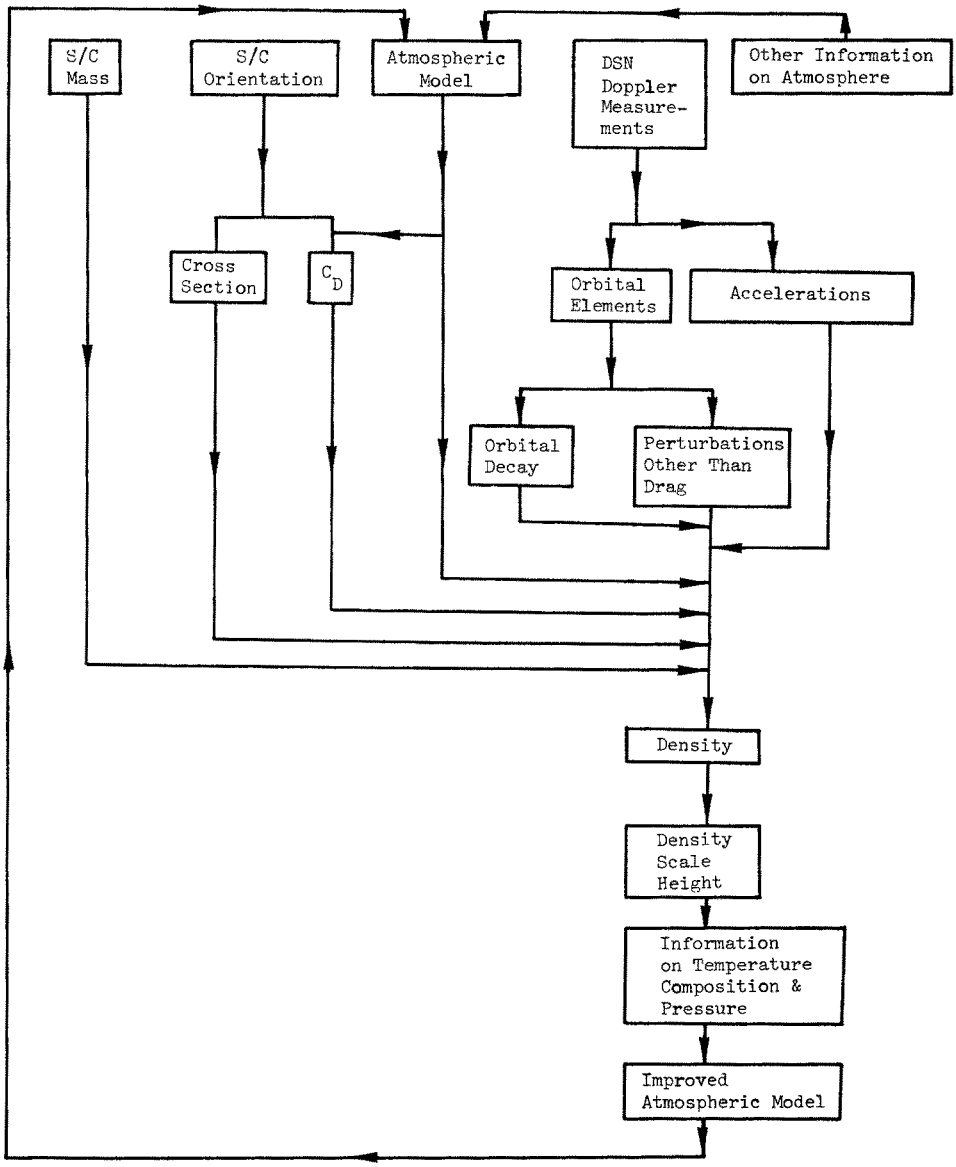

Fig. 34. (OAD). Block diagram of Atmospheric Drag experiment.

ments and then determining how the semi-major axis or orbital period changes with time. The time rate of change of the orbital inclination will also be studied. The small effects of perturbations other than drag will then be calculated and subtracted from the total changes to yield the changes due to drag.

Once the orbital decay rate due to drag is determined this information is combined with the information on spacecraft mass, spacecraft cross-section and

drag coefficient, the atmospheric model and the orbital elements to yield the atmospheric density.

The periapsis altitude of the Orbiter changes with time. By studying how the density changes with measurement altitude, the density scale height can be determined. It is expected that at altitudes below about 200 km, in addition to obtaining densities from changes in mean elements, it may be possible to measure the shorter term drag accelerations on the spacecraft as it approaches and recedes from periapsis. Using this secondary method it may be possible to observe short-term variations in density scale height.

From knowledge of the density and density scale height, information can be inferred concerning the temperature and composition of the atmosphere which in turn yields information about pressure gradients and flow patterns.

From changes in inclination of Earth satellites information has been obtained about the rotation of the upper atmosphere. Possible changes in the inclination of the Pioneer Venus Orbiter will be studied to try to establish evidence of a super rotation of the planet's upper atmosphere.

The drag measurements will be used to obtain an improved atmospheric model which will then be fed back into the original atmospheric model so that improved density determinations can be obtained. Information from previous experiments as well as other experiments aboard the Orbiter and probes will also be used to improve the model of the upper atmosphere.

It is planned that these drag measurements will be obtained throughout the mission yielding information on diurnal, and semi-annual variations, long- and short-term variations with solar activity, variations with the solar wind and perhaps information on the super rotation of the upper atmosphere.

31. Orbiter Internal Density Distribution Experiment (OIDD) —R. Phillips/JPL

Pioneer Venus Orbiter gravity data for the OIDD Experiment will be derived from radiometric tracking data provided by the Deep Space Network (DSN). The tracking data will be obtained via a coherent loop that includes Earth-based transmitting and receiving stations plus a transponder on the spacecraft. An S-band signal (approximately 2.2 GHz), referenced to a stable oscillator, is transmitted from a ground antenna, received by the spacecraft transponder and retransmitted coherently back to the ground antenna. The received signal and transmitted signal are then heterodyned to yield a Doppler frequency which is proportional to the spacecraft-antenna range-rate. This Doppler frequency is continuously monitored and counted at fixed time intervals. The count value is proportional to the two-way range change between the spacecraft and the tracking station over the count interval.

The count values are the basic input data to an Orbit Determination Program (ODP). Line-of-sight gravity data may be derived by finding the least-squares

mean orbital fit to this Doppler data. The fit residuals may be differentiated to yield a least-squares biased estimate of the line-of-sight gravity vector. In such a procedure, other components contributing to spacecraft acceleration, such as atmospheric drag, solar radiation pressure, and attraction of other solar system bodies, must be modeled.

Alternatively, the gravity field of Venus can also be parameterized and combined with these other model effects to yield an overall fit to the Doppler data. Such a procedure starts with an initial estimate of the gravity field parameters and predicted spacecraft ephemeris and iterates to an acceptable least-squares solution.

Examples of parameterization of the Venus gravity field to be used are spherical harmonics, point masses, and continuous surface density distributions.

The gravity models when cmbined with topographic data from the ORAD provide the basic information for studying the internal density distribution of Venus. The Green's function for gravitational attraction is integrated over the topography to yield the *Bouguer correction* to the gravity data. When this correction is made, the remaining *Bouguer gravity* is due to internal density variations only. The correction may be made to the gravity field model, or, the Bouguer correction can be incorporated into the ODP to yield a direct least-squares solution for the Bouguer gravity.

32. Orbiter Celestial Mechanics Experiment (OCM) — I. Shapiro/MIT

This radio science experiment makes use of the spacecraft's radio-tracking system as well as the on-board radar system (ORAD). A modulated carrier signal at a frequency of about 2.2 GHz is transmitted from an antenna of the Deep Space Network (DSN) on the Earth towards the spacecraft. On the spacecraft, a radio transponder receives the signal, and retransmits it towards the ground, after multiplication of the frequency by the factor 240/221. In the absence of noise, the phase of the retransmitted signal would be coherent with that received by the spacecraft. This multiplication is necessary to allow the spacecraft to detect the incoming signal while continuing to transmit towards the ground. The returned signal is heterodyned to produce a video signal, offset by a known frequency from that due to the Doppler shift alone. The Doppler shift can thus be reconstructed from this 'biased Doppler' video signal.

The signal transmitted from the ground station and the heterodyne, or local-oscillator, signal used in the ground station for reception are both controlled by the same, stable atomic-frequency standard in this 'closed-loop' tracking system. The three DSN sites, one each in Goldstone, California; Madrid, Spain; and Canberra, Australia, will probably rely on hydrogen-maser frequency standards for this purpose in 1978–79. The long-term ($\geq$1000 s) frequency drift of such standards should be under 1 part in 10^{13} and, thus, during the typical signal round-trip time of 1000 s, this drift should introduce an error in the Doppler shift

of under 0.2 mHz. The short-term fluctuations introduced by the standards in the received signal will be under 1 mHz.

The cycles of the biased Doppler signal are counted at the ground station and the count sampled at uniform intervals, usually 1 second apart. Since the probability of even a single cycle 'slip' during the period ($\simeq 8$ to 12 hr) that the spacecraft is in the view of a given station is very low, the changes in phase delay of the propagation of the signal from ground to spacecraft and back again can be monitored for this entire period.

The time-tagged differences between uniformly spaced samples of the cycle count, divided by the time interval between the epochs of the samples and corrected for the effects of the known frequency offset, constitute the primary ('Doppler') data available for investigations that depend mainly on the orbit of the spacecraft. These Doppler data represent the history of the rate of change of the range between ground and spacecraft and hence contain information on the spacecraft accelerations. These, in turn, are caused by the physical characteristics of interest such as the mass and gravitational field of Venus and the atmosphere of Venus, which exerts a drag force on the spacecraft. The propagation medium also affects the Doppler data directly and characteristics of this medium can thereby also be obtained through analysis of the Doppler data. For occasions just preceding and just following the occultation of the spacecraft by Venus, the ordinary radio-tracking system will be supplemented at the relevant DSN site by an 'open-loop' recording system (see, for example, Howard *et al.* (1974)) that provides a wide-band signal for more elaborate studies of the atmosphere and ionosphere of Venus, possible because the ray path passes quite near to the surface during the periods surrounding occultations. The open-loop system is also useful to record the signals transmitted by the spacecraft in its free-running mode, controlled by a stable on-board crystal oscillator. This free-running condition exists for the time period between emergence of the spacecraft from occultation and the establishment of a two-way 'lock' between the ground transmissions and the transponded signals from the spacecraft.

In summary, the radio-tracking system, supplemented by open-loop recording, provides data suitable primarily for the detailed study of the gravitational field of Venus and of its atmosphere and ionosphere.

References

Bennett, W. H.: 1950, *J. Appl. Phys.* **21,** 143.

Brace, L. H., Theis, R. F., and Dalgarno, A.: 1973, *Radio Science* **8,** 341.

Brace, L. H., Carignan, G. R., and Findlay, J. A.: 1971, *Space Research XI,* p. 1080–1005, Akademie–Verlag, Berlin.

Bridge, H. S., Lazarus, A. J., Snyder, C. W., Smith, E. J., Davis, L., Jr., Coleman, P. J., Jr., and Jones, D. E.: *Science* **158,** 1669.

Bridge, H. S., Lazarus, A. J., Scudder, J. D., Ogilvie, K. W., Hartle, R. E., Asbridge, J. R., Bame, S. J., Feldman, W. C., and Siscoe, G. L.: 1974, *Science* **183,** 1291.

Brinton, H. C., Scott, L. R., Pharo, M. W., III, and Coulson, J. T.: 1973, *Radio Science* **8,** 323.
Cloutier, P. A., McElroy, M. B., and Michel, F. C.: 1969, *J. Geophys. Res.* **74,** 6215.
Counselman, C. C.: 1976, *Ann. Rev. Astron. Astrophys.* **14** (in press).
Counselman, C. C., Hinteregger, H. F., and Shapiro, I. I.: 1972, *Science* **178,** 607.
Counselman, C. C., Hinteregger, H. F., King, R. W., and Shapiro, I. I.: 1973, *Science* **181,** 772.
Dolginov, Sh. Sh., Yeroshenko, Ye. G., and Zhuzgov, L. N.: 1973, *J. Geophys. Res.* **78,** 4779.
Gringauz, K. I., *et al.*: 1973, *J. Geophys. Res.* **78,** 5808.
Hartle, R. E., Bauer, S. J., and Wu, C. S.: 1973, IAGA Bulletin No. 34 (KYOTO, 569.
Hoegy, W. R. and Wharton, L. E.: 1973, *J. Appl. Phys.* **44,** 5365.
Houghton, J. T. and Taylor, F. W.: 1974, *J. Atmos. Sci.* **32,** 620.
Howard, H. T. *et al.*/20 authors): 1974, *Science* **183,** 1297.
Johnson, C. Y.: 1960, *Encyclopedia of Spectroscopy*, ed. by G. L. Clark, 587–598, Reinhold, New York.
King, R. W.: 1975, *Precision Selenodesy via Differential Very-Long-Baseline Interferometry*, Ph.D. thesis, Mass. Inst. of Technology, Cambridge. 173 pp.
Knudsen, W. C.: 1966, *J. Geophys. Res.* **71,** 4669.
McKibben, D. D., Wolfe, J. H., Collard, H. R., Savage, H. F., Molari, R.: 1972, *Space Science Instrumentation* (Submitted for publication).
Nier, A. O., Potter, W. E., Hickman, D. R., and Mauersberger, K.: 1973, *Radio Science* **8,** 271.
Nier, A. O., Potter, W. E., Kayser, D. C., and Finstad, R. G.: 1974, *Geophys. Res. Letters* **1,** 197.
Oyama, V. I.: 1972, *Icarus* **16,** 167.
Pettengill, G. H., Shapiro, I. I., and Prinn, R. G.: 1975, "Preliminary Experiment Description: Differenced Long-Baseline Interferometric Tracking of Entry Probes to Determine Wind Speeds in the Venus Atmosphere", report under NASA contract NAS 2-7994, Mass. Inst. of Technology, Cambridge. 54 pp.
Rodriguez, P. and Gurnett, D. A.: 1975, *J. Geophys. Res.* **80,** 19.
Scarf F. L.: 1970, *Space Sci. Rev.* **11,** 234.
Scarf, F. L., Crook, G. M., Green, I. M., and Virobik, P. F.: 1968, *J. Geophys. Res.* **73,** 6665.
Scarf, F. L., Green, I. M., and Crook, G. M.: 1971, *Cosmic Electrodyn.* **1,** 496.
Schubert, G., *et al.* (12 authors): 1976, *Space Sci. Rev.*, this issue.
Spencer, N. W., Brace, L. H., Carignan, G. R., Taeusch, D. R., and Niemann, H.: 1965, *J. Geophys. Res.* **70,** 2665.
Spenner, K. and Dumbs, A.: 1974, *J. Geophys.* **40,** 585.
Spreiter, J. R., Summers, A. L., and Rizzi, A. W.: 1970, *Plan. Space Sci.* **18,** 1281.
Taylor, F. W., Houghton, J. T., Peskett, G. D., Rodgers, C. D., and Williamson, E. J., *Appl. Opt.* **11,** 135.
Trinks, H.: 1975, *Geophys. Res. Letters* **2,** 99.
Wallis, M. K.: 1972, *Cosmic Electrodyn.* **3,** 45.
Woo, R., Ishimaru, A., and Kendall, W. B.: 1974, *J. Atmos. Sci.* **31,** 1698.
Woo, R.: 1975a, *J. Atmos. Sci.* **32,** 1084.
Woo, R.: 1975b, *Astrophys. J.* **201,** 238.
Woo, R. and Yang, F. C.: 1976, *J. Geophys. Res.*, in press.
Woo, R., Yang, F. C., Yip, K. W., and Kendall, W. B.: 1976a. *Astrophys. J.*, in press.
Woo, R., Yang, F. C., and Ishimaru, A.: 1976b, *Astrophys. J.*, in press.